AN EXPERIMENTAL AND ANALYTICAL VIBRATION STUDY OF A RING-STIFFENED CYLINDRICAL SHELL STRUCTURE WITH VARIOUS SUPPORT CONDITIONS

by John L. Sewall, Robert R. Clary,
and Sumner A. Leadbetter

Langley Research Center
Langley Station, Hampton, Va.

AN EXPERIMENTAL AND ANALYTICAL VIBRATION STUDY OF A

RING-STIFFENED CYLINDRICAL SHELL STRUCTURE

WITH VARIOUS SUPPORT CONDITIONS

By John L. Sewall, Robert R. Clary,
and Sumner A. Leadbetter

Langley Research Center
Langley Station, Hampton, Va.

AN EXPERIMENTAL AND ANALYTICAL VIBRATION STUDY OF A

RING-STIFFENED CYLINDRICAL SHELL STRUCTURE

WITH VARIOUS SUPPORT CONDITIONS

By John L. Sewall, Robert R. Clary,
and Sumner A. Leadbetter
Langley Research Center

SUMMARY

This paper reports an experimental and analytical vibration study of two ring-stiffened cylindrical shell models used in search of a suitable design for the test chamber of the Langley low-frequency noise facility. One of these models consisted of a steel cylindrical shell with steel rings of I-beam cross section welded to the outside surface and spaced in six nearly equal intervals along the length. The other model was formed from this single-wall model by fastening an outer shell on the outer flanges of the rings.

Natural frequencies and mode shapes of both models were measured under various end and longitudinal support conditions. Installation of the outer shell resulted in slight increases in frequency that were not considered sufficient to warrant the use of an outer shell on the full-scale test chamber. Despite the bothersome apparent existence of multiple resonances having the same mode shape, experimental results show that the natural frequencies increase as the degree of end fixity increases, although the frequency increases were not as great as desired because of insufficiencies in the end clamping action in the configurations tested.

Application of a Rayleigh type of vibration analysis gave frequencies that were in generally satisfactory agreement with measured frequencies of both models for low shell vibration modes except for cases where discrepancies between calculated and measured frequencies can be attributed to insufficient end clamping action. The calculations also indicated that strain energy terms involving the torsional stiffness and the bending and stretching stiffnesses due to cross coupling between longitudinal and circumferential strains could be omitted without appreciably affecting the frequencies of the lower modes.

INTRODUCTION

During the preparation of design specifications for a large cylindrical test chamber for the Langley low-frequency noise facility, particular consideration was given to the vibration characteristics of the test chamber. This

consideration, which is unusual for permanent structures, involved the requirement that the minimum natural frequency of the test chamber be as far beyond the proposed noise-frequency test range of the facility as possible. The effort to satisfy such a requirement led to the construction and testing of a vibration model together with analytical shell vibration studies on the model in support of vibration design studies of the full-scale structure. Preliminary estimates of shell frequencies on unstiffened shells indicated the need for discrete stiffeners, at least in the form of rings, and on the basis of these estimates, the model was built to approximately 1/10th scale, with seven equally spaced ring stiffeners and tested under various support conditions. As a result of vibration tests and calculations on the model, together with the full-scale analytical design studies, longerons as well as rings were incorporated into the final design of the facility; however, time did not permit the building and testing of another model to evaluate this design fully.

The purpose of this paper is to report the results of both the experimental and analytical vibration studies of the ring-stiffened model, particularly with regard to two problems which were encountered in the course of the investigation and which must also be dealt with in determining the vibration characteristics of built-up shell structural components in aircraft and space flight vehicles. One of these problems is concerned with the support conditions at the ends of the structure, and the other problem has to do with the manner in which ring and longeron stiffeners are accounted for in a vibration analysis involving these elements.

With regard to the first of these problems, the literature is replete with vibration studies of cylindrical shell structures having simply supported ends. However, relatively little effort is reported for other support or end conditions approximating those either for the test chamber of the noise facility or in aircraft and space vehicle structures. References 1 to 3 are examples of theoretical studies of unstiffened cylindrical shells with various combinations of clamped and supported ends. Theory and experiment are correlated in reference 4 for an unstiffened clamped-clamped shell, in reference 5 for clamped-free shells, and to a limited extent in reference 6 for free-free shells, but generally speaking theoretical and experimental studies, correlated or not, are conspicuously lacking for end conditions other than simply supported.

The problem of accounting for the effects of ring and longeron stiffeners has been dealt with in the literature in two ways. In one approach, a certain amount of shell is assumed to act with a stiffener in bending, and the actual amount chosen is based either on experimental stiffness measurements (refs. 7 and 8) or on theoretical considerations related to static stress distributions (refs. 9 to 12). Vibration analyses written so as to receive this kind of stiffness input are reported in references 13 and 14, both of which are based on the assumption that the actual stiffened cylindrical shell can be replaced by a homogeneous shell of constant thickness with equivalent stiffness properties. In reference 13 the measured stiffnesses obtained in references 7 and 8 are used, and in reference 14 the stiffnesses are calculated by use of beam and plate theories.

Another method for allowing for the effects of ring and longeron stiffeners involves first calculating the energies of stiffeners and shell separately and

then linearly combining them in the derivation of the frequency equation. This approach is followed in references 12 and 15 for stiffened cylindrical shells with simply (or freely) supported ends. Reference 12 reports a vibration analysis of a ring-stiffened cylindrical shell in which additional modes are introduced to obtain a more accurate representation of the mode shape of the shell between rings. In reference 15 longerons as well as rings are provided for, and the shell bending energy is considered negligibly small in comparison with the energies of rings and longerons. A general modal expansion involving higher modes is used in reference 15, and coupling effects due to stiffener spacing are discussed with regard to certain combinations of these modes.

With due cognizance of the merits of references 12 to 15, correlation between theory and experiment was nevertheless considered insufficient with regard to the two foregoing methods of treating the effects of stiffeners for the design problem of the noise facility. Accordingly, the construction and vibration testing of a model was deemed necessary along with complementary analytical studies, and the results obtained from this effort are considered worth reporting for the benefit of designers confronted with similar situations both in land-based and aerospace structures.

The Rayleigh type of equivalent shell analysis of reference 14 was chosen for this investigation and was extended to include end conditions other than simply (or freely) supported. Provision is also made for estimating the effects of a double-walled configuration, and detailed stiffness and mass expressions are given in an appendix. The support conditions approximated in the test program of the model included free ends, one end clamped and the other free, both ends clamped, one end clamped and the other end having an internal restraint against radial deflection, and the case of the model clamped both at one end and along longitudinal supports. Frequency calculations were made for all but the last two of the support conditions just mentioned and also for the model with assumed simply supported ends. The effects of mounting an outer shell so that the rings were between the two shells were explored both in the vibration tests and in the frequency calculations. The effects on the model's vibration characteristics of two different methods of fabrication, particularly the manner by which the shells were attached to the ring stiffeners, were also studied experimentally.

The experimental work is reported first, followed by the presentation of the analysis and by comparisons of experimental and analytical results. In addition to the vibration data on the ring-stiffened configuration, measured frequencies on an unstiffened free-ended cylindrical shell are reproduced from reference 16 for comparison with frequencies calculated by the analysis of the present paper.

The main text concludes with a brief discussion of the effect on frequency of eliminating from the strain energy certain stiffness terms, particularly those involving coupling between longitudinal and circumferential deformations.

a mean radius of equivalent cylindrical shell (see appendix following eq. (A6))

a_i radius to middle surface of inner shell

a_o radius to middle surface of outer shell

A_L cross-sectional area of longeron

A_F cross-sectional area of ring

A_{Sx} cross-sectional area of shells acting with longerons in longitudinal stretching (see eq. (A1))

A_{Ss} cross-sectional area of shells acting with rings in circumferential stretching (see eq. (A1))

$a_{mn}(t)$ generalized coordinate for longitudinal motion

$b_{mn}(t)$ generalized coordinate for circumferential motion

$c_{mn}(t)$ generalized coordinate for radial motion

d distance between inner and outer shells

C_{jk}, D_{jk} stretching and bending stiffnesses, respectively (see text following eq. (1))

E_{LS} Young's modulus of elasticity for shells and longerons

E_F Young's modulus of elasticity for rings

$f = \dfrac{\omega}{2\pi}$ circular frequency, cps

h_S shell thickness

I_F area moment of inertia of ring about its own centroidal axis normal to plane of ring

I_L area moment of inertia of longeron about its own centroidal axis in longitudinal bending

I_{Lx} area moment of inertia of longeron about centroidal surface of shell-longeron combination (see eq. (A2))

I_{Fs} area moment of inertia of ring about centroidal surface of shell-ring combination (see eq. (A2))

I_{Sx} area moment of inertia of shells effective in longitudinal bending about centroidal surface of shell-longeron combination (see eq. (A1))

I_{Ss} area moment of inertia of shells effective in circumferential bending about centroidal surface of shell-ring combination (see eq. (A1))

L length of orthogonally stiffened cylindrical shell structure

L_s, L_x circumferential and longitudinal lengths of repeating section, respectively (see fig. 10 and appendix)

m_A mass per unit surface area of equivalent cylindrical shell

m longitudinal mode number

n circumferential mode number or number of circumferential waves

N_m eigenvalue of beam mode approximation (see table VI)

r_s, r_x location of centroidal surfaces of ring-shell and longeron shell combinations, respectively (see fig. 10 and eq. (A3))

s circumferential coordinate (see fig. 10)

t time

T kinetic energy

U potential or strain energy

u, v, w longitudinal, circumferential, and radial displacements, respectively (see fig. 10)

x longitudinal coordinate (see fig. 10)

$X_m(x)$ mth longitudinal mode shape

$$X_m{}'(x) = \frac{d}{dx} X_m(x)$$

y_F, y_L distances from underside of inner shell to centroidal axes of ring and longeron, respectively (see fig. 10)

z radial coordinate, positive toward axis of shell structure (see fig. 10)

β = 0 or 1   depending on whether the shells are detached from or attached to the appropriate stiffeners between rings and between longerons (see appendix)

γ_m coefficient in beam mode approximation (see table VI)

ω angular frequency, radians/sec

ϕ_s central angle of repeating section (see fig. 10)

ν Poisson's ratio

ρ_F mass density of ring

ρ_{LS} mass density of shell and longeron

ρ_S mass density of shell

ζ effective length factor (see eq. (7))

$\lambda_{11}, \lambda_{12}, \ldots \lambda_{33}$ determinant elements of frequency equation (eq. (6))

Subscripts:

i   associated with inner shell

j,k   identify the stretching and bending stiffnesses (see eq. (1) and appendix)

m   associated with mth longitudinal mode shape where m = 0, 1, 2, . . .

n   associated with nth circumferential mode shape where n = 0, 1, 2, . . .

o   associated with outer shell

s   denotes differentiation with respect to s; also identifies circumferential direction

x   denotes differentiation with respect to x; also identifies longitudinal direction

Double subscripts on β:

is,os   associated with attachment of ring to inner or outer shell, respectively

ix,ox   associated with attachment of longeron to inner or outer shell, respectively

Bars over lengths denote effective lengths (see eqs. (A4)); also nondimensional longitudinal coordinate, i.e., $\bar{x} = x/L$. Dots indicate derivatives with respect to time. Primes denote derivatives with respect to x.

EXPERIMENTAL INVESTIGATION

Model

The ring-stiffened cylindrical shell model used for the vibration studies reported in this paper was constructed of 18-gage (0.049 inch) steel sheets and of steel I-beams that were approximately 1/10 scale modified 8WF67 (wide flange) sections. As shown in figure 1(a), the model was 29.42 inches long with an inside diameter of 28.20 inches, and the I-beams were formed into seven ring stiffeners spaced in nearly equal intervals along the length of the model. The inner radius of the ring was 14.15 inches and the outer radius, 15.03 inches. Cross-sectional dimensions of the ring stiffeners are given in figure 1(b). The dimensions shown in figure 1 were scaled down from those of the test chamber of the Langley low-frequency noise facility by the ratio 1/10.2 and were based on a preliminary design of the test chamber.

For initial vibration tests, the rings were spotwelded along their inside flanges to the outside surface of the 18-gage inner shell, and upon completion of these tests, another 18-gage steel sheet was first riveted and then spotwelded to the outer flanges of the rings as indicated in figure 1(a). For convenience in identification, the initial ring-stiffened configuration is referred to as the single-wall model and the subsequent configurations as the riveted double-wall model or the welded double-wall model as the case may be.

Test Equipment and Application

Two types of vibrators were used, in separate tests, to excite the natural frequencies of the model by forcing it in a radial direction. One of these was an electromagnetic shaker capable of producing a maximum zero-to-peak force of 25 pounds, and the other was an air shaker of the type described in reference 17.

The instrumentation used in conjunction with the electromagnetic shaker is shown in figure 2. The oscillator signal was used to drive the shaker and was also applied to an electronic digital counter and to the horizontal deflection plates of a cathode-ray oscilloscope. A crystal accelerometer was hand-held in various locations on the surface of the model, and the accelerometer signals were applied to the vertical deflection plates of the oscilloscope. The resulting pattern on the oscilloscope, commonly referred to as a Lissajous figure, indicated the phase and frequency relations of the oscillator and accelerometer signal. In some of the vibration tests the accelerometer signals were monitored to obtain relative radial deflections or mode shapes.

In tests with the air shaker, natural frequencies were obtained by varying the shaking frequency until maximum (or resonant) responses were determined by

fingertip touch on the surface of the model. Nodes were also located by finger-
tip touch.

Test Procedure

Vibration data on the model were obtained for several support conditions
that included varying degrees of end fixity. First to be tested was the free-
ended or free-free model and next was the model with one end clamped (or fixed)
and the other free. Vibration tests were then conducted with a special support
installed in the free end of the fixed-free model and with both ends fixed.
Tests were also conducted with the model mounted on two longitudinal supports
in an attempt to simulate actual support conditions for the test chamber of the
Langley low-frequency noise facility. The electromagnetic shaker was used for
all of the configurations and, in addition, the air shaker was used for the
free-free configuration. The complete test program is summarized in the fol-
lowing table according to support conditions and single- or double-wall
configurations:

Support conditions	Wall configuration
Free-free and fixed-free ends	Single-wall; riveted double-wall; welded double-wall
Fixed ends	Single-wall; riveted double-wall
Fixed-supported ends	Welded double-wall
Fixed-free ends, longitudinal supports	Single-wall; welded double-wall
Fixed-supported ends, longitudinal supports	Welded double-wall

It should be noted that the term "fixed" in this table is used, at least
in the experimental part of the paper, more for convenience of identification
than it is to denote a condition of true fixity or clamping.

Free-free end conditions.- The single-wall model was suspended vertically
by three cords equally spaced around the circumference of the model to simulate
free-free end conditions. In order to determine whether the position or mass
of the driving elements of the shaker had any appreciable effect on the vibra-
tion modes of the model, two different types of shakers were used and were
located in different positions on the model. Vibration tests were conducted
first with the electromagnetic shaker attached to the middle ring stiffener or
the end ring stiffener, and then with the air shaker located at an end ring
stiffener. Results of these tests, given in table I, indicate negligible

effects on the natural frequencies of the model due either to the location of the shaker or to the mass of the moving coil of the electromagnetic shaker. On the basis of these tests, the electromagnetic shaker was used for the remainder of the test program and was located to obtain maximum response for any mode and support condition.

The riveted and welded double-wall models were also hung in the same manner as that used for the single-wall model, and natural frequencies were obtained with the electromagnetic shaker attached to one of the end rings.

Fixed-free end conditions.- The single-wall model with one end fixed and the other end free is shown in figure 3(a). One end of the model was clamped to a massive foundation structure, hereafter referred to as the "backstop," by means of 14 clamping dogs equally spaced around the circumference of the end ring stiffener. Vibration tests were conducted with the electromagnetic shaker attached either to the middle ring stiffener or to the ring stiffener at the free end.

The fixed end of the double-wall fixed-free model, shown in figure 3(b), was clamped to the backstop by means of a heavy steel ring that was bolted to the end ring stiffener with another steel ring inserted between inner and outer walls to act as a spacer, as shown in figure 4(a). The shaker was attached to the free end of the model.

Fixed-supported end conditions.- The end conditions designated as fixed supported were obtained by mounting an aluminum "spider" in the free end of the fixed-free welded double-wall model. The spider consisted of a circular hub drilled and tapped around its circumference to receive eight equally spaced circular rods bearing at their outer ends against the inside of the inner shell. The threaded ends of the rods at the hub were secured by means of lock screws across the threads in order to maintain the restraint provided by the rods against localized radial motion of the free end of the model during vibration. The shaker was attached near the middle ring stiffener by means of a vacuum coupler, described in reference 18.

Fixed-fixed end conditions.- The single-wall model with both ends fixed is shown in figure 5(a). One end was clamped to the backstop in the manner previously described for the fixed-free end conditions. A steel plate 3/4 inch thick was clamped to the ring stiffener at the other end of the model and to a horizontal face of the backstop by means of two reinforced angles. The shaker was attached to the middle ring stiffener.

As shown in figure 5(b), the fixed-fixed double-wall model was mounted on the backstop in the manner just described for the single-wall model except for the modification, shown in figure 4(b), of the end attached to the reinforced angles. The shaker was attached near the middle ring stiffener by means of a vacuum coupler as before.

Longitudinal supports.- Figure 6 shows one of the configurations used to simulate actual support conditions of the cylindrical test chamber of the Langley low-frequency noise facility. Both single-wall and double-wall models

9

were mounted, in fixed-free end conditions, on longitudinal wood supports secured by means of C-clamps to two I-beam rails running longitudinally inside the model. The rails, which were 3WF57 sections, were located so that the included angle at the axis of the model was 54°. This angular spacing closely corresponds to the locations of the foundation piers of the full-scale test chamber. The shaker was attached near the middle of the model as before.

In another configuration simulating support conditions for the Langley low-frequency noise facility, the spider was installed in the free end of the fixed-free double-wall model in an effort to obtain data representative of full-scale vibration characteristics of the test chamber with both ends closed.

Experimental Results

The experimental vibration data obtained for the single-wall and double-wall ring-stiffened cylindrical shell models of figures 1, 3, 4, 5, and 6 are presented in tables I to V and in figures 7 and 8. Dashes in the tables for certain combinations of m and n indicate that no resonant frequencies were found for these modes. Discussion of these results is concerned with the effects of the various support conditions beginning with free ends, the effects of double-wall configurations, and with the existence of more than one resonant frequency for the same mode shape.

The modes are identified by integer indices m and n. For the free-ended model, m denotes the number of circumferential nodes, whereas for all the other support conditions considered in this paper m is one more than the number of circumferential nodes between the ends of the model, the end supports or restraints not counting as nodes. The circumferential mode number n denotes the number of circumferential waves and is always half the number of longitudinal nodes for any given mode. Values of $n \geqq 2$ are associated with modes involving noncircular distortions with 4 or more longitudinal node lines and are designated as shell modes of vibration. Values of $n < 2$ do not represent shell modes since the cylindrical cross section remains circular or undistorted during vibration.

Tables I to V indicate that, with the exception of the fixed-ended and special boundary conditions involving longitudinal supports (tables IV and V, respectively), the minimum frequencies measured, irrespective of end conditions, were shell frequencies for $n = 2$.

Effects of free-ends.- Lowest frequencies of the entire test program were obtained for the free-ended models (tables I and II) with $m = 0$ and 1 which denote ring bending modes with $2n$ longitudinal node lines. When $m = 0$, the ends of the model moved in phase, and when $m = 1$, the ends moved out of phase, and there was a circumferential node line between the ends. One feature of the free-free modes which distinguishes them from those obtained with other end fixities is that for a given value of n, there is little difference between the frequency for $m = 0$ and the frequency for $m = 1$ over the range of n-values covered in the test program. This behavior is in agreement with that observed by Grinsted in reference 16 for an unstiffened free-ended cylindrical

shell of considerably smaller radius and length than the radius and length of the present model. Grinsted's results, which are reproduced in figure 9, covered a wider range of modes than was possible in the present study and clearly indicate another distinguishing characteristic of the free-free shell modes, namely, that the frequencies for $m = 0$ and 1 approach zero as n approaches zero, instead of increasing rapidly from some minimum frequency as for $m \geqq 2$ and, as has been found by other writers (for example, ref. 2), for various degrees of end fixity with $m \geqq 1$.

Free-free frequency trends similar to those of reference 16 and the present paper are reported by Heckl in reference 6 for $m = 0, 2, 3, \ldots$ in experiments on unstiffened cylindrical shells of greater length-diameter ratios than those of reference 16 or of the present model. However, Heckl's results do not include frequencies for $m = 1$.

Effects of support conditions.- As was expected, an increase in the degree of restraint in the different support conditions other than free-free resulted in corresponding increases in the lower mode frequencies. For example, comparison of tables I and II with table III shows that the fixed-free frequencies for $m = 1$, $n = 2$ are on the order of 50 percent to 70 percent higher than the corresponding free-free frequencies for $m = 0$ and $m = 1$. It is also evident from table III that the frequency of the fixed-free model for $m = 1$, $n = 2$ was more than doubled because of the presence of the spider in the free end. Highest frequencies at the low n-values of 2 and 3 were measured for the fixed-fixed model (table IV), and a mode shift for minimum frequency from $n = 2$ to $n = 3$ is indicated for the riveted double-wall configuration.

Further comparison of the frequencies in tables I to V indicates that as n increased, the distinction between various degrees of end fixity, including free ends, became less important. This tendency is well enough established from the works of other investigators, notably Arnold and Warburton in reference 2.

With regard to the effects of longitudinal supports, comparison of tables III and V indicates about a 40-percent increase in frequency due to these supports for the single-wall model and $m = 1$, $n = 2$. However, further effects are not clearly discernible because of the existence of at least two resonant frequencies for the same mode shape.

Results of mode-shape measurements.- Despite the efforts at clamping illustrated in figures 3 to 5, truly clamped end conditions could not be achieved in this investigation. True or ideal end fixity of a cylindrical shell structure requires that the shell displacements u, v, and w, together with the slope of the radial displacement $\partial w/\partial x$, be zero at the end. The extent to which these conditions were realized in the present study is indicated by the measured radial mode shape components presented in figures 7 and 8. These data were obtained by normalizing accelerometer outputs along the length of the model with respect to accelerometer outputs corresponding to maximum radial deflections.

Figure 7 applies to the double-wall model with one end fixed and the other end either free or supported by the spider. With or without the spider in the

free end, the mode-shape trends appear to be about the same and indicate zero radial deflection but nonzero slope at the fixed end. The approach to zero slope at $\bar{x} = 1$ is in contrast to the arbitrary slope allowed with either free or simply supported ends of beams. These trends are discussed further in connection with theoretical results which include frequency calculations based on the trigonometric modal approximation identified as supported-sliding in the figure.

Mode-shape data for the single-wall model with both ends fixed is shown in figure 8 for three natural frequencies. (The first subscript on f denotes m and the second subscript n.) Small deflections were obtained at the ends of the model (figs. 8(a) and 8(b)), and the deflections at the end fixed to the reinforced angles were larger than the deflections at the other end. Nonzero slopes at both ends are also indicated, although these trends are harder to see because of the zig-zag variations which are attributed to the stiffening effects of the rings. These data are discussed further in connection with calculated frequencies based on the theoretical mode shapes shown in the figure.

Effects of outer-wall installations.- In an effort to increase the frequencies of the model substantially, an outer shell was attached to the outer flanges of the rings. First, the outer shell was riveted to the rings at uniformly spaced intervals around the circumference. Next, the outer shell was spotwelded to the rings between rivets. Frequencies of the free-ended double-wall model are listed in table II for both riveted and welded outer shell attachments. Except for the mode $m = 1$, $n = 2$, riveting the outer shell to the rings had the effect of reducing the frequencies by about $1\frac{1}{4}$ percent for $m = 1$, $n = 3$ to 8 percent for $m = 0$, $n = 4$. With the addition of the spotwelds, these frequency reductions were recovered and the frequencies increased still further. However, the net gain in frequency as a result of riveting and then spotwelding was less than 5 percent over the range of modes covered in the test program.

The effects of the outer shell on the frequencies of the fixed-free model are shown in table III. The stiffening effect of spotwelding the outer shell is also evident from the $8\frac{1}{2}$ - percent increase in frequency over the frequency of the riveted configuration (at $m = 1$, $n = 4$). On the basis of these results, the installation of an outer shell on the stiffened full-scale test chamber did not seem worthwhile.

Existence of multiple resonances.- An interesting phenomenon indicated by data of tables I to V and hindering separate consideration of other effects is the existence of at least two resonant natural frequencies having similar nodal patterns. Double resonances are reported in reference 19 for cylindrical shells and in reference 20 for double-conical sandwich disks. In a more general investigation reported in reference 21, this behavior is shown to be not uncommon in elastic bodies of revolution and to be due to structural deviation from rotational symmetry inherent in fabrication and in the materials themselves.

In the present investigation, not only two but also three or more resonant frequencies were obtained for the same mode shape for most of the configurations

tested. This is particularly true of the fixed ended single-wall model where as many as 7 resonant frequencies occurred in a 129 cycle per second range for one mode. (See table IV for $m = 1$, $n = 3$.) Six resonances were observed for the welded double-wall model with fixed-free end conditions and mounted on longitudinal supports. (See table V for $m = 1$, $n = 2$.) The only configurations for which multiple resonances were noticeably absent were the riveted double-wall models for free-free and fixed-free end conditions. (See tables II and III.) Riveted connections may have provided structural damping sufficient to eliminate the additional resonances from these models. However, this possibility cannot be argued for the riveted double-wall fixed-fixed model, inasmuch as double resonances occurred in all but one of the modes obtained. (See table IV.)

ANALYTICAL INVESTIGATION AND CORRELATION WITH EXPERIMENT

Method of Analysis

The calculated frequencies presented in this paper were obtained by application of the Rayleigh type vibration analysis of reference 14 which is extended to include end conditions other than simply supported and to allow for a double-walled configuration with ring and longeron stiffeners between the two walls. As shown in reference 14, the method basically involves an equivalent shell concept wherein the actual stiffened structure is approximated by a uniformly thick shell with equivalent stiffnesses calculated on the basis of both beam and plate theories. In the present investigation the shell is considered subdivided into curved sections of equal size as shown in figure 10, where each of these sections is seen to consist of an inner and an outer shell separated by mutually perpendicular ring and longeron stiffeners.

The essential features of the vibration analysis of this configuration are presented in this section and in the appendix. The analysis is a straightforward application of Lagrange's equations to the harmonic motions of a stiffened cylindrical shell structure in the longitudinal, circumferential, and radial directions. Beginning with the strain energy in the form derived in reference 14, a general cubic frequency equation is obtained in which the longitudinal components of the mode shapes in the three directions just mentioned can be varied in accordance with a desired set of end conditions. As for the circumferential components of the mode shapes, the trigonometric approximations commonly used in other shell analyses are also used here.

Strain energy.- The strain energy used for the orthotropic configuration shown in figure 10 is given by

$$U = \frac{1}{2} \int_0^{2\pi a} \int_0^L \left[D_{11}w_{xx}^2 + D_{22}\left(w_{ss} + \frac{1}{a}v_s\right)^2 + 2D_{12}w_{xx}\left(w_{ss} + \frac{1}{a}v_s\right) \right.$$

$$+ D_{66}\left(w_{xs} + \frac{1}{a}v_x\right)^2 + C_{11}u_x^2 + C_{22}\left(v_s - \frac{1}{a}w\right)^2$$

$$\left. + 2C_{12}u_x\left(v_s - \frac{1}{a}w\right) + C_{66}(v_x + u_s)^2 \right] dx\,ds \qquad (1)$$

where D_{jk} and C_{jk} are bending and stretching stiffnesses, respectively, and where the subscript 11 identifies the longitudinal stiffness; the subscript 22, the circumferential stiffness; and the subscript 12, the stiffness due to cross-coupling between longitudinal and circumferential deformations. The torsional stiffness is indicated by D_{66} and the middle-surface shearing stiffness by C_{66}. Displacements in the longitudinal, circumferential, and radial directions are represented by u, v, and w, respectively, as shown in figure 10, and the subscripts x and s denote partial differentiation with respect to the longitudinal and circumferential coordinates.

The stiffnesses D_{jk} and C_{jk} are calculated from a knowledge of the elastic and geometric properties of the repeating section in figure 10. Detailed expressions for these stiffnesses are given in the appendix wherein the stiffness contributions of the ring and longeron are calculated from beam theory and the stiffness contributions of the shells from plate theory. Also, in the expressions for both the circumferential bending stiffness of the ring-shell combination and the longitudinal bending stiffness of the longeron-shell combination, only part of the shell length between stiffeners is assumed to be effective. Further discussion of this approximation is given in a later section of the paper.

In passing, it may be noted here, as in reference 14, that D_{jk} and C_{jk} could be alternatively expressed in terms of the thickness of the equivalent shell and the elastic constants in the stress-strain relations for an orthotropic shell. This approach has been used in references 7, 8, and 13 in the experimental determination of stiffnesses of ring-shell combinations.

Modal approximations.- The longitudinal, circumferential, and radial motions of the shell configuration of figure 10 are assumed to be given by

$$\left. \begin{aligned} u(x,s,t) &= a_{mn}(t)\,X_m'(x)\,\cos\frac{ns}{a} \\[6pt] v(x,s,t) &= b_{mn}(t)\,X_m(x)\,\sin\frac{ns}{a} \\[6pt] w(x,s,t) &= c_{mn}(t)\,X_m(x)\,\cos\frac{ns}{a} \end{aligned} \right\} \qquad (2)$$

where $a_{mn}(t)$, $b_{mn}(t)$, $c_{mn}(t)$ are generalized coordinates, m and n are integers identifying the longitudinal and circumferential components of the mode shape, and $X_m(x)$ is the mth longitudinal component which is chosen so as to satisfy a desired set of end conditions. For example, in the case of a simply supported shell structure in which the ends are free to move longitudinally but must remain circular in cross section, the function usually selected is

$$X_m(x) = \sin \frac{m\pi x}{L} \tag{3}$$

where m = 1, 2, . . . and L is the length of the shell.

The choice of the derivative $X_m'(x)$ in the first of equations (2) evolved from physical considerations based on the experimentally observed behavior of the longitudinal components of the two lowest sets of free-free mode shapes (that is, for m = 0 and 1). In the case of m = 0, for example, circumferential bending is the predominant deformation involved in the motion, and the mode shapes must be chosen so that all longitudinal motion is eliminated completely and the effect of the circumferential stretching stiffness (C_{22} in eq. (1)) is minimized. When m = 1, the mode shape must be such that the circumferential bending stiffness D_{22} is retained and the middle-surface shear term C_{66}, along with the circumferential stiffness C_{22}, is minimized. Although a more rigorous justification for $X_m'(x)$ for end conditions in general is not readily available, certain basic developments in thin-shell theory in the treatises of Love and Rayleigh (refs. 22 and 23) indicate that the functional dependence of u on the longitudinal coordinate x is of lower order than that of v and w.

Functions for end conditions other than simply supported are more or less complicated than equation (3) depending on the mode shape and end conditions involved. A complete list of the functions used in the present study is given in table VI(a). With the exception of the two lowest sets of free-free modes, which clearly involve rigid-body longitudinal components (m = 0 and 1), the tabulated functions are based on the elastic properties of uniform beams for the end conditions considered. Most of these functions are seen to have the form of the characteristic function (or eigenfunction) obtained from the exact solution of the differential equation for beam vibration. The parameters N_m and γ_m apply to a particular mode shape and set of end conditions, and numerical values of these parameters are given in table VI(b) which is taken from reference 24. Table VI(a) also includes a simple parabolic approximation to the lowest flexible clamped-free longitudinal mode shape (that is, for m = 1).

Frequency equation.- To obtain the frequency equation for this study, the strain energy given by equation (1) was used along with the following expression for kinetic energy:

$$T = \frac{m_A}{2} \int_0^{2\pi a} \int_0^L \left(\dot{u}^2 + \dot{v}^2 + \dot{w}^2 \right) dx \; ds \qquad (4)$$

where dots over the displacements denote differentiation with respect to time and m_A is the mass per unit surface area of the equivalent shell or the mass per unit area of the repeating section of the cylindrical shell as given in the appendix. The equations of motion, given by Lagrange's equations, are

$$\left. \begin{aligned} \frac{d}{dt}\left(\frac{\partial T}{\partial \dot{a}_{mn}}\right) - \frac{\partial T}{\partial a_{mn}} + \frac{\partial U}{\partial a_{mn}} &= 0 \\[2ex] \frac{d}{dt}\left(\frac{\partial T}{\partial \dot{b}_{mn}}\right) - \frac{\partial T}{\partial b_{mn}} + \frac{\partial U}{\partial b_{mn}} &= 0 \\[2ex] \frac{d}{dt}\left(\frac{\partial T}{\partial \dot{c}_{mn}}\right) - \frac{\partial T}{\partial c_{mn}} + \frac{\partial U}{\partial c_{mn}} &= 0 \end{aligned} \right\} \qquad (5)$$

With the use of equations (1), (2), and (4) in equations (5) and the assumption of simple harmonic motion, the following frequency equation is obtained in the usual manner by setting the determinant of the coefficients of the generalized coordinates a_{mn}, b_{mn}, and c_{mn} equal to zero for nontrivial solutions:

$$\begin{vmatrix} \lambda_{11} - \Delta \int_0^L (X_m')^2 dx & \lambda_{12} & \lambda_{13} \\[2ex] \lambda_{21} & \lambda_{22} - \Delta \int_0^L X_m^2 dx & \lambda_{23} \\[2ex] \lambda_{31} & \lambda_{32} & \lambda_{33} - \Delta \int_0^L X_m^2 dx \end{vmatrix} = 0 \qquad (6)$$

where $\Delta = \dfrac{a^2 m_A \omega^2}{C_{11}}$, ω is the natural frequency, and where

$$\lambda_{11} = a^2 \int_0^L (X_m'')^2 dx + n^2 \frac{C_{66}}{C_{11}} \int_0^L (X_m')^2 dx$$

16

$$\lambda_{12} = \lambda_{21} = na\left[\frac{c_{12}}{c_{11}} \int_0^L X_m X_m{}'' dx - \frac{c_{66}}{c_{11}} \int_0^L (X_m')^2 dx\right]$$

$$\lambda_{13} = \lambda_{31} = -a\frac{c_{12}}{c_{11}} \int_0^L X_m X_m{}'' dx$$

$$\lambda_{22} = n^2\left(\frac{D_{22}}{a^2 c_{11}} + \frac{c_{22}}{c_{11}}\right)\int_0^L X_m{}^2 dx + a^2\left(\frac{D_{66}}{a^2 c_{11}} + \frac{c_{66}}{c_{11}}\right)\int_0^L (X_m')^2 dx$$

$$\lambda_{23} = \lambda_{32} = n\left[-\left(\frac{n^2 D_{22}}{a^2 c_{11}} + \frac{c_{22}}{c_{11}}\right)\int_0^L X_m{}^2 dx\right.$$

$$\left. + a^2\left(\frac{D_{12}}{a^2 c_{11}} \int_0^L X_m X_m{}'' dx - \frac{D_{66}}{a^2 c_{11}} \int_0^L (X_m')^2 dx\right)\right]$$

$$\lambda_{33} = \frac{a^2 D_{11}}{c_{11}} \int_0^L (X_m{}'')^2 dx + \left(\frac{n^4 D_{22}}{a^2 c_{11}} + \frac{c_{22}}{c_{11}}\right)\int_0^L X_m{}^2 dx$$

$$- (na)^2\left(2\frac{D_{12}}{a^2 c_{11}} \int_0^L X_m X_m{}'' dx - \frac{D_{66}}{a^2 c_{11}} \int_0^L (X_m')^2 dx\right)$$

Evaluated forms of the integrals appearing in equation (6) are listed in table VI(a) for the various end conditions considered in this investigation. Integrals for the exact uniform-beam modes were taken from reference 25 in which are listed evaluated forms of integrals for a wide range of end conditions.

Analytical Results and Comparison With Experiment

Frequencies calculated by use of equation (6) are presented and compared with experiment in tables VII and VIII and in figures 11 to 15 for the ring-stiffened cylindrical shell configuration of figure 1. The experimental results used in this comparison for the double-wall model apply to the case of the outer wall both riveted and welded to the rings. Equation (6) is also applied to the small unstiffened cylindrical shell tested by Grinsted in reference 16, and theoretical and experimental frequencies are compared in figure 9. Except for the free-free cases with $m = 0$ and $m = 1$, most of the assumed longitudinal mode shapes used in the calculations were obtained from the exact solution

of the differential equation for beam vibration. The frequencies based on these mode shapes are designated as beam mode in figure 13 when being distinguished from those based on the parabolic approximation to lowest longitudinal fixed-free, or cantilever, mode shape. In the discussion of these results, consideration is given (1) to the length of shell between rings that is assumed to be effective in circumferential bending; (2) to the effects of various end conditions on frequency; (3) to the effects of ring stiffeners and other modal approximations; and (4) to the effects on frequency of eliminating certain stiffnesses from the strain-energy expression given by equation (1). In the discussion for each set of end conditions, consideration is given to the effects of extreme values of longitudinal bending stiffness on the calculated frequencies of the double-wall model.

Effective length approximation.- As previously noted, only part of the shell length between stiffeners is assumed to be effective in determining the bending stiffness of ring- and longeron-shell combinations in the vibration analysis used in this study. In application of equation (6) to the ring-stiffened shell configuration, most of the frequency calculations were based on the effective length approximation given in reference 12 and applied herein to the inner and outer shell separately by the relations

$$
\left.
\begin{aligned}
\bar{L}_{x,i} &= \frac{2}{\zeta_i} \\[2mm]
\bar{L}_{x,o} &= \frac{2}{\zeta_o}
\end{aligned}
\right\}
\tag{7}
$$

where $\zeta_i = \sqrt[4]{\dfrac{3(1 - \nu^2)}{a_i{}^2 h_{S,i}^2}}$ for the inner shell and $\zeta_o = \sqrt[4]{\dfrac{3(1 - \nu^2)}{a_o{}^2 h_{S,o}^2}}$ for the

outer shell. According to this approximation, only 27.2 percent of the length of the inner shell and 28.05 percent of the length of the outer shell between rings were considered to be effective in the circumferential bending stiffness of the ring-shell combination. As may be seen from tables VII and VIII and figures 11 to 15, the calculated frequencies based on these approximations were everywhere higher than the experimental frequencies and were in particularly good agreement with experiment for the two lowest free-free longitudinal modes (m = 0 and m = 1) of the single-wall model at low values of n.

In order to determine how sensitive the calculated frequencies were to the effective shell approximation, some calculations were made with all the shell length between rings assumed effective in bending, and the results are given in table VII for the two lowest free-free modes and in figure 13 for the cantilever end conditions. It is evident that reducing shell effectiveness caused more of a frequency reduction for the double-wall configuration than for the single-wall configuration. Moreover, there was a much smaller frequency reduction for the cantilever end conditions than for the two lowest free-free modes at values of n associated with minimum shell frequencies. For m = 0, reducing the shell effectiveness from 100 percent to 27.2 percent and 28.05 percent for the inner

18

and outer shells, respectively, caused a frequency drop of about 56 percent for the double-wall model and 17 percent for the single-wall model. For m = 1, the frequency reduction for the single-wall model was about the same as that for m = 0 but the reduction for the double-wall model was about 21 percent at n = 2 and tended toward higher percentages with increasing values of n. Reducing shell effectiveness for the cantilever configuration resulted in a drop in minimum frequency of about $7\frac{1}{2}$ percent for the double-wall model and $4\frac{1}{4}$ percent for the single-wall model.

Free-free end conditions of the ring-stiffened model.- Calculated frequencies for the ring-stiffened free-free cylindrical shell structures are presented and compared with measured frequencies in tables VII and VIII and in figures 11 and 12. Better agreement between theory and experiment is clearly evident for m = 0 and m = 1 than for m = 2, and also for the single-wall model as compared with the double-wall model. Furthermore, the discrepancy between theory and experiment tends to increase as n increases and is particularly large for m = 2, n = 4.

For the double-wall model (fig. 11), this behavior is attributed to the fact that the calculated frequencies are based on a longitudinal bending stiffness that is too high because of the assumption of perfect separation between inner and outer shells with both shells bending about a common (or equivalent) neutral surface between them. Although this assumption is inherent to the equivalent-shell concept of the analysis used in this study, it is obviously inconsistent with reality when longerons or other means of shell separation are absent, because then each shell tends to bend longitudinally about its own middle surface. This separate bending of the shells cannot be strictly accounted for within the scope of the analysis, but its effect may be approximated by simply putting β_{1x} and β_{0x} equal to zero in equation (A1) in the appendix to eliminate the inertia transfer terms which exist because of the equivalent neutral surface. This approximation reduces to a minimum not only the longitudinal bending stiffness D_{11} but also the cross-coupling bending stiffness D_{12} and the torsional stiffness D_{66} and can have a large effect on the calculated frequency, as is evident from the trends of the dashed curves in figure 11 for m = 1 and 2. As may be seen, these frequencies for m = 1 are essentially coincident with those for m = 0 and are in very good agreement with experiment. For m = 2, n = 4, the calculated frequency based on the maximum longitudinal bending stiffness decreased by nearly a factor of 2 to within 13 percent of the experimental frequency due to this approximation. It may be noted that a similar approximation would be required for a double-shell configuration stiffened only by longerons, although in this case only the circumferential bending stiffness D_{22} would be affected.

Other possible causes of the discrepancies between theory and experiment in figures 11 and 12 include imperfections in the fabrication of the model that could have more of an effect on higher modes than on lower modes, inadequacies of the modal approximations, and transverse shear effects (in the radial direction) which were not included in the strain energy expression. (See eq. (1).) In regard to the modal approximations, for example, the assumed longitudinal

mode shape for m = 2, based on the exact solution for the vibration of a uniform free-free beam, does not account for the localized effect of the rings. Moreover, the simple trigonometric representation of the circumferential mode shape does not take into account structural dissymmetries along the shell circumference.

Free-free end conditions of an unstiffened model.- An opportunity for a closer view of the merits of the modal approximations alone is afforded in figure 9 where measured shell frequencies observed by Grinsted in reference 16 on a small unstiffened free-free shell are compared with calculated shell frequencies for a wide range of modes. The comparison indicates that the longitudinal uniform beam modes and the circumferential trigonometric functions chosen in this study offer satisfactory approximations to the frequencies of an unstiffened free-free shell for m = 2 and the first several values of n. The increasing separation between theory and experiment with increasing values of m and n is regarded as a consequence of the application of a Rayleigh type vibration analysis with each of the three shell displacements represented by just one pair of mode shapes, as in equation (2).

Ring-bending considerations.- When m = 0 and $X_O = 1$ (see table VI(a)), equation (6) reduces to a quadratic equation with the first row and column of the determinant eliminated. Frequencies calculated by this reduced equation are compared in table VIII both with measured frequencies and with those calculated by use of Timoshenko's frequency equation for ring bending, derived in reference 26. The two sets of calculated frequencies agree to within 3 percent for the double-wall model, 8 percent for the single-wall model, and to within 5 percent for the small unstiffened shell. Moreover, the ring frequencies are in better agreement with measured frequencies than are those obtained from equation (6). The small differences between the two sets of calculated frequencies are attributed mainly to the effect of Poisson's ratio which is present in the reduced quadratic form of equation (6) but not in Timoshenko's equation for ring bending alone.

Fixed-free end conditions of ring-stiffened model.- Calculated frequencies for the ring-stiffened cylindrical shell structures, each with one end fixed and the other end free, are compared with measured frequencies in figure 13 for the lowest longitudinal mode, m = 1. Considerably better agreement between theory and experiment is evident here than for the first flexible free-free mode (m = 2), and somewhat better agreement can be noted for the single-wall model than for the double-wall model. As in the free-free case, the discrepancy between measured and calculated frequencies tends to increase as n increases. For the double-wall model (fig. 13(a)), the effect on the calculated frequencies of reducing the longitudinal bending stiffness to a minimum is seen to be considerably smaller than was the case for the free-free model. At n = 3, the calculated frequency based on this approximation is about 10 percent closer to experiment than that based on the maximum longitudinal bending stiffness.

Although the reasoning advanced to explain the possible causes of the disagreement between theory and experiment in the free-free case can be applied to the fixed-free case, additional consideration must be given to the end conditions, particularly in regard to end fixity. In this respect, it is noted

in figure 13 that the measured frequencies for $n = 2$ agree better with the calculated frequencies on the curves labeled "inextensional theory" than they do with those on the next higher curves. These lower curves were obtained by applying equation (6) with terms involving the longitudinal strain component u_x omitted from the strain-energy expression. (See eq. (1).) The better agreement of experiment with inextensional theory at $n = 2$ suggests that the end clamping indicated in figure 3 may not have been sufficient to achieve the zero slope condition required of a truly clamped end. As previously noted in the discussion of experimental results, further indication of this possibility is given by the nonzero, fixed-end slope of the measured longitudinal mode shapes shown in figure 7 which also shows that the slope of the free end approaches zero rather than remaining arbitrary as required of a truly free-end condition. A longitudinal mode shape approximating that of figure 7 is given by the trigonometric function identified as supported-sliding in table VI(a), and frequency calculations based on this approximation are shown in figure 14 to give results that are substantially closer to experiment than are those based on the cantilever longitudinal mode shape. For $n = 2$, the calculated frequencies for the two different sets of end conditions differ by about 28 percent for both single- and double-wall models. For the supported-sliding double-wall model (fig. 14(a)), reducing to a minimum the longitudinal bending stiffness resulted in decreases in the calculated frequencies by about the same amounts as for the fixed-free model.

Fixed-fixed end conditions of the ring-stiffened model.- Calculated and measured frequencies for both double- and single-walled, ring-stiffened, fixed-fixed cylindrical shells are compared in figure 15 for the lowest longitudinal mode, $m = 1$. Reducing the longitudinal bending stiffness to a minimum clearly had a greater effect on the calculated frequencies of the double-wall fixed-fixed model than for either the fixed-free or supported-sliding model. For $n = 4$ and 5, this approximation reduced the calculated frequencies by about 30 percent, and brought the theory and experiment that much closer together. Again the same reasoning advanced to explain the possible causes of the discrepancy between theory and experiment in the free-free case can be applied here but with more emphasis given to deficiencies in the end clamping noted earlier in the discussion of experimental results. The fact that the calculated frequencies based on simply supported ends for $m = 1$ and the single-wall structure appear to agree better with measured frequencies than do those based on purely clamped ends suggests the existence of the same weakness in end fixity . that was noted for the fixed end of the fixed-free end conditions. The measured mode shape data of figure 8 lend strength to this explanation by indicating nonzero slopes as well as deflections of the ends of the model. For the minimum frequency at $n = 3$, the calculated simply supported frequency of the single-wall model was 26 percent closer to the measured frequency than was the calculated clamped-clamped frequency.

Simply supported end conditions of the ring-stiffened model.- As a matter of additional interest, the calculated simply supported frequencies of the single-wall model shown in figure 15 are also reproduced in figures 12 and 13(b) for comparison with the free-free and fixed-free frequencies. Figure 12 shows that the minimum frequency of the ring-stiffened shell with simply supported ends was $63\frac{1}{2}$ percent lower than the minimum frequency for the first free-free

elastic mode (that is, m = 2). On the other hand, figure 13(b) shows that the minimum simply supported frequency was not only 65 percent higher than the minimum cantilever or fixed-free frequency but was also shifted to a higher mode (that is, from n = 2 to n = 3).

Effects of rings.- In the absence of measured frequencies on the unstiffened single-wall model, some calculations were made for both the free-free and fixed-free unstiffened model, and the results are presented in figures 12 and 13(b). The stiffening effect of the rings is evident in the large increases in slope of the curves of frequency plotted against n for the two lowest free-free modes in figure 12 and in the 210-percent increase in frequency of the minimum unstiffened clamped-free mode in figure 13(b). This large increase in minimum frequency was accompanied by a shift in circumferential mode from n = 5 to n = 2. Although the unstiffened free-free calculations were not carried to the point of minimum frequency for m = 2, the trend in figure 12 is clearly similar to that shown for the clamped-free case in figure 13(b), the circumferential mode being shifted from n > 5 to n = 3. For values of n less than those for minimum frequency, the rings clearly have a mass effect which is evident in the reduction of the frequency (by as much as about 28 percent for the free-free structure at m = 2, n = 2).

Other modal approximations.- As previously noted, most of the frequency calculations presented in this paper were based on longitudinal mode shapes obtained from the exact solution of the differential equation for beam vibration. Some calculations for the fixed-free case were based on a simple parabolic approximation for m = 1, and comparison of these results with those based on the beam-mode shape in figure 13(b) shows that the parabolic approximation gives a minimum frequency that is about 19 percent higher than that given by the beam-mode shape. Since this difference is in the direction of poorer agreement with experiment, the comparison of the two sets of calculations with experiment indicates the need for choosing longitudinal modal functions that more nearly satisfy the end conditions in order to obtain more accurate theoretical frequencies.

The zig-zag variations of the measured longitudinal mode shape in figure 8 suggest that the smooth functions that have been used in the theory be replaced or modified by functions intended to reproduce these localized variations, which are attributed to the stiffening effects of the rings. This approach has been used in reference 12 in which the inter-ring shell deformation is represented by two additional degrees of freedom each with a single-cycle sinusoidal approximation to the longitudinal mode shape between rings. The shell length between rings is assumed to be fully effective in the circumferential bending stiffness of the ring-shell combination. Frequencies calculated for a ring-stiffened cylindrical shell with 14 equally and closely spaced rings between the ends were reduced by about 2 percent at the minimum frequency and by no more than 11 percent at higher values of n because of the inter-ring deformation. Although this shell structure was quite different from the one dealt with in the present paper, this effect of inter-ring deformation on frequency in reference 12 has the same order of magnitude as that due to reducing the amount of shell assumed to be effective in circumferential bending of the ring-shell configuration of the present paper. This observation implies

that the mode-shape modification used in reference 12 can be regarded as essentially equivalent, as far as the effect on frequency is concerned, to leaving the overall mode shape unchanged and assuming the shell between rings only partially effective in circumferential bending, as has been done in the equivalent shell concept used in the present study.

Effect of coupling and torsional stiffnesses.- It should be noted that the basic assumptions and corresponding simple expressions given in the appendix for D_{12}, C_{12}, D_{66}, and C_{66} are based on orthotropic shell theory for homogenous structures and may therefore be questionable approximations for built-up structures having relatively few longeron and/or ring stiffeners, as was the case with the model used in the present investigation. However, the effect of these terms on frequency may be small enough to justify their omission from the strain energy. In order to determine how far such a simplification could be carried in the present investigation, some frequency calculations were performed first with the coupling stiffnesses C_{12} and D_{12} omitted, next with the torsional stiffness D_{66} also omitted, and finally with all three of these stiffnesses together with the middle-surface shearing stiffness C_{66} omitted. Results of these calculations showed a negligible reduction in frequency due to the elimination of C_{12}, D_{12}, and D_{66} for the single-wall model with free-free, cantilever, clamped-clamped, and simply supported end conditions. This effect is illustrated for the free-free model in figure 12 where the dashed curve is no more than 3 percent below the solid curve representing the inclusion of all stiffnesses. In contrast to this small effect, very large reductions in frequency were obtained when C_{66} was also omitted from the calculations, and for the cases with varying degrees of end fixity, the trend in frequencies was essentially the same as that of the inextensional theory in figure 13.

Calculations with $C_{12} = D_{12} = D_{66} = 0$ were also performed for the free-free unstiffened cylindrical shell of reference 16, and the results are compared in figure 9 with the calculations in which all stiffnesses were included. For $m = 1$, the elimination of these three stiffness terms had a negligible effect on frequency, as was the case for the ring-stiffened model, but, as may be seen, the frequency reduction tended to increase appreciably for higher longitudinal modes ($m \geq 2$). Thus, only for the lower longitudinal modes does the effect on frequency of eliminating the coupling and torsional stiffnesses appear to be small enough for these stiffnesses to be eliminated. However, it may also be noted that for the higher longitudinal modes, omission of these stiffness terms resulted in noticeably improved agreement between theory and experiment, particularly in the vicinity of minimum frequency.

CONCLUDING REMARKS

This paper reports an experimental and analytical vibration study of a ring-stiffened cylindrical shell model that was built and tested to obtain information for designing the large cylindrical test chamber of the Langley low-frequency noise facility to have a minimum natural frequency as far beyond

the proposed noise-frequency test range as possible. The model, which was built with seven equally spaced rings on the basis of preliminary frequency calculations of unstiffened shells, was vibration-tested for various end and longitudinal support conditions, first as a single-wall model with the rings mounted externally to the shell and then with an outer shell secured to the outer flanges of the rings. Installation of the outer shell resulted in slight increases in frequency that were not considered sufficient to warrant the use of an outer shell on the full-scale test chamber. Frequency calculations were performed for several end-support conditions by application of a Rayleigh type vibration analysis which takes into account the effects of ring and longeron stiffeners through the concept of an equivalent shell in which only part of the shell in the vicinity of a stiffener is assumed to be effective in bending of the stiffener-shell combination.

Results of the investigation show that this type of vibration analysis can serve as a useful design tool for predicting lower natural frequencies of built-up cylindrical shell structures for a wide range of end-support conditions. For free-free, fixed-free, and fixed-fixed end conditions, measured frequencies were in generally satisfactory agreement with calculated frequencies for which the shell contribution to the circumferential bending stiffness of each ring-shell combination was based on 27 percent to 28 percent of the shell length between rings.

Improved agreement between theory and experiment was obtained for the double-wall configuration when the calculated longitudinal bending stiffness was reduced to a minimum in order to simulate the actual lack of longerons between inner and outer shells and the consequent tendency of each shell to bend about its own middle surface. This stiffness reduction resulted in large decreases in frequency - on the order of 30 percent and higher - for the free-free and fixed-fixed models, but for the fixed-free end conditions, the frequency reduction was much smaller - less than 10 percent.

Much of the discrepancy between measured and calculated frequencies for the fixed-free and fixed-fixed models can be attributed to the lack of sufficient end clamping action to approach the condition of true (or ideal) fixity which can be assumed in the analysis but could not be practicably attained during the test program.

A dominant feature of the experimental results of this investigation was the existence of multiple resonances which hindered isolation of other effects, such as those due to longitudinal supports and to spotwelding as well as riveting the outer shell to the ring flanges. This behavior, in which more than one resonant frequency exists for the same nodal pattern, is similar to the double resonance phenomenon which has been shown by other investigators to occur in elastic bodies of revolution because of structural deviations from rotational symmetry. In the present study, as many as seven resonances for the same nodal pattern were observed over a 129-cycle-per-second frequency range.

Analytical results alone showed large increases in frequency due to the stiffening effect of the rings. Frequency calculations also showed that the

coupling and torsional stiffnesses could be eliminated from the strain energy without appreciably affecting the frequencies of the lower longitudinal modes.

Langley Research Center,
　　　　National Aeronautics and Space Administration,
　　　　　　　Langley Station, Hampton, Va., April 21, 1964.

APPENDIX

BENDING AND STRETCHING STIFFNESSES AND MASS PER UNIT SURFACE AREA

OF ORTHOGONALLY STIFFENED CYLINDRICAL SHELL

This appendix contains expressions that are extensions of those given in reference 14 for calculating the bending and stretching stiffnesses and the mass per unit area $\left(D_{jk}, \quad C_{jk}, \quad \text{and} \quad m_A, \quad \text{respectively}\right)$ of the double-walled, orthogonally stiffened cylindrical shell section shown in figure 10. The stiffnesses are given first and are followed by the areas, flexural moments of inertia, and centroids of the ring- and longeron-shell configuration of the repeating section for which both beam and plate theories are employed. In reference 14 the shell length between longerons is assumed to be fully effective in calculating the longitudinal bending stiffness of the longeron-shell combination, whereas the shell length between ring stiffeners is assumed to be only partially effective in calculating the circumferential bending stiffness of the ring-shell combination. As can be seen in the inertia expressions, provision is made for considering the shell partially effective in longitudinal as well as circumferential bending for both inner and outer shells. Provision is also made for the case of either shell detached from either ring or longeron stiffener except at ring-longeron intersections. This feature follows that of reference 14 in which the shell can be either continuously attached to or completely detached from the ring stiffeners between longerons.

The expression for mass per unit area of the repeating section follows those for areas and flexural moments of inertia.

Stiffnesses

In the stiffness expressions given in the following table, the rings are assumed to have a negligible effect on the longitudinal bending, stretching, and the coupling stiffnesses $\left(D_{12}, \quad C_{12}\right)$, and the longerons are assumed to have a negligible effect on the circumferential bending and stretching stiffnesses. Torsion and middle-surface shear are assumed to be carried only by the longeron-shell combination.

In the following table, E_{LS} is Young's modulus for longerons and shells, ν is Poisson's ratio for the shells, E_F is Young's modulus of the rings, and L_X and L_S are lengths of the repeating section in axial and circumferential directions, respectively. The length $L_S = \phi_S a$ where ϕ_S is the central angle of the repeating section (see fig. 10) and a is the radius of the equivalent shell. The A terms denote cross-sectional areas of stiffeners and shells effective in stretching, and the I terms denote area (or flexural) moments of inertia of stiffeners and shells effective in bending.

Identification of stiffness	Bending stiffness, D_{jk}	Stretching stiffness, C_{jk}
Longitudinal	$D_{11} = \dfrac{E_{LS}}{L_s}\left(I_{Lx} + \dfrac{I_{Sx}}{1 - \nu^2}\right)$	$C_{11} = \dfrac{E_{LS}}{L_s}\left(A_L + \dfrac{A_{Sx}}{1 - \nu^2}\right)$
Circumferential	$D_{22} = \dfrac{1}{L_x}\left(E_F I_{Fs} + \dfrac{E_{LS} I_{Ss}}{1 - \nu^2}\right)$	$C_{22} = \dfrac{1}{L_x}\left(E_F A_F + \dfrac{E_{LS} A_{Ss}}{1 - \nu^2}\right)$
Longitudinal-circumferential coupling	$D_{12} = \nu D_{11}$	$C_{12} = \nu C_{11}$
Torsional	$D_{66} = 2(1 - \nu)D_{11}$	
Middle-surface shearing		$C_{66} = \dfrac{1 - \nu}{2}\, C_{11}$

Detailed expressions for these structural properties follow, first for the shells and then for the rings and longerons.

$$A_{Sx} = h_{S,i}L_{s,i} + h_{S,o}L_{s,o}$$

$$A_{Ss} = \left(h_{S,i} + h_{S,o}\right)L_x$$

$$I_{Sx} = \overline{L}_{s,i}\,\frac{h_{S,i}^3}{12} + \overline{L}_{s,o}\,\frac{h_{S,o}^3}{12} + \beta_{ix}\overline{L}_{s,i}h_{S,i}\left(r_x + \frac{h_{S,i}}{2}\right)^2$$

$$+ \beta_{ox}\overline{L}_{s,o}h_{S,o}\left(d + \frac{h_{S,o}}{2} - r_x\right)^2$$

$$I_{Ss} = \overline{L}_{x,i}\,\frac{h_{S,i}^3}{12} + \overline{L}_{x,o}\,\frac{h_{S,o}^3}{12} + \beta_{is}\overline{L}_{x,i}h_{S,i}\left(r_s + \frac{h_{S,i}}{2}\right)^2$$

$$+ \beta_{os}\overline{L}_{x,o}h_{S,o}\left(d + \frac{h_{S,o}}{2} - r_s\right)^2$$

$$(A1)$$

for the shells, and

$$
\left.
\begin{aligned}
I_{Lx} &= I_L + A_L\left(y_L - h_{S,i} - r_x\right)^2 \\[2em]
I_{Fs} &= I_F + A_F\left(y_F - h_{S,i} - r_s\right)^2
\end{aligned}
\right\}
\tag{A2}
$$

for the longerons and rings, where

$$
\left.
\begin{aligned}
r_x &= \frac{A_L\left(y_L - h_{S,i}\right) - \beta_{ix}\bar{L}_{s,i}\dfrac{h_{S,i}^2}{2} + \beta_{ox}\bar{L}_{s,o}h_{S,o}\left(d + \dfrac{h_{S,o}}{2}\right)}{A_L + \beta_{ix}\bar{L}_{s,i}h_{S,i} + \beta_{ox}\bar{L}_{s,o}h_{S,o}} \\[2em]
r_s &= \frac{A_F\left(y_F - h_{S,i}\right) - \beta_{is}\bar{L}_{x,i}\dfrac{h_{S,i}^2}{2} + \beta_{os}\bar{L}_{x,o}h_{S,o}\left(d + \dfrac{h_{S,o}}{2}\right)}{A_F + \beta_{is}\bar{L}_{x,i}h_{S,i} + \beta_{os}\bar{L}_{x,o}h_{S,o}}
\end{aligned}
\right\}
\tag{A3}
$$

Inner and outer shell thicknesses are denoted by $h_{S,i}$ and $h_{S,o}$, respectively, d is the distance between the shells (see fig. 10), A_L and A_F are cross-sectional areas of longeron and ring, I_L and I_F are area moments of inertia of longeron and ring about their own centroidal axes, and y_L and y_F are the distances from the centroidal axes of longeron and ring to the underside of the inner shell. The barred quantities denote effective lengths of the shell in longitudinal and circumferential bending that are related to the lengths of the repeating section by

$$
\left.
\begin{aligned}
\bar{L}_{s,i} &\leqq L_{s,i} \\[1em]
\bar{L}_{s,o} &\leqq L_{s,o} \\[1em]
\bar{L}_{x,i} &\leqq L_x \\[1em]
\bar{L}_{x,o} &\leqq L_x
\end{aligned}
\right\}
\tag{A4}
$$

where $L_{s,i} = \phi_s a_i$ and $L_{s,o} = \phi_s a_o = \phi_s\left(a_i + d + \dfrac{h_{S,i} + h_{S,o}}{2}\right)$, a_i being the radius to the middle surface of the inner shell. (For a cylindrical shell configuration stiffened only by rings, $\phi_s = 2\pi$.) The β terms in equations (A1) to (A3) are each zero or one depending on whether the shells are detached from or attached to the appropriate stiffeners between ring-longeron intersections (for example, $\beta_{is} = 0$ or 1, as in reference 14, depending on

whether the inner shell is detached from or attached to the ring except at the ring-longeron intersection).

For double-wall shells stiffened by either rings or longerons, but not both, the elimination of the ring or longeron moments of inertia (eqs. (A2)), depending on which stiffener is omitted, is not alone sufficient to account for the correct bending stiffness in the direction of the missing stiffener. The presence of the third and fourth terms in I_{Sx} and I_{Ss} of equations (A1) implies perfect separation between inner and outer shells, bending taking place about a common neutral surface between them. However, without the ring or longeron or any other means of separation, each shell tends to bend about its own middle surface. Although this separate bending cannot be accurately accounted for within the scope of the present analysis, the effect may be reasonably approximated by simply putting the appropriate β-values equal to zero to eliminate the inertia transfer terms. Thus, for a ring-stiffened shell, β_{ix} and β_{ox} should be made equal to zero, and for a longeron-stiffened shell, β_{is} and β_{os} should be made equal to zero.

For the unstiffened cylindrical shell, $\phi_S = 2\pi$, $h_{S,o} = d = 0$, $\overline{L}_{s,i} = L_{s,i} = L_s$, $\overline{L}_{x,i} = L$, equations (A2) are eliminated, and the longitudinal and circumferential stiffnesses in the foregoing table reduce to

$$\left. \begin{aligned} D_{11} = D_{22} &= \frac{E_{LS} h_{S,i}^3}{12\left(1 - \nu^2\right)} \\[2mm] C_{11} = C_{22} &= \frac{E_{LS} h_{S,i}}{1 - \nu^2} \end{aligned} \right\} \tag{A5}$$

Mass Per Unit Area

The average mass per unit area of the double-walled, orthogonally stiffened cylindrical shell of figure 10 is given by

$$m_A = \frac{\rho_{LS} L_x \left(h_{S,i} L_{s,i} + h_{S,o} L_{s,o} + A_L \right) + \rho_F A_F L_s}{L_s L_x} \tag{A6}$$

where ρ_{LS} is the mass density of shells and longeron, ρ_F the mass density of the rings, and $L_s = \phi_S a$ with $a = a_i + \dfrac{h_{S,i} + r_x + r_s}{2}$. For an unstiffened cylindrical shell, equation (A6) reduces to $m_A = \rho_S h_{S,i}$.

REFERENCES

1. Yu, Yi-Yuan: Free Vibrations of Thin Cylindrical Shells Having Finite Lengths With Freely Supported and Clamped Edges. Jour. Appl. Mech., vol. 22, no. 4, Dec. 1955, pp. 547-552.

2. Arnold, R. N., and Warburton, G. B.: The Flexural Vibrations of Thin Cylinders. Proc. (A) Inst. Mech. Eng. (London), vol. 167, no. 1, 1953, pp. 62-74.

3. Baron, Melvin L., and Bleich, Hans H.: The Dynamic Analysis of Empty and Partially Full Cylindrical Tanks. Part I - Frequencies and Modes of Free Vibration and Transient Response by Mode Analysis. DASA No. 1123A (Contract DA-29-044-XZ-557), Defense Atomic Support Agency, May 1959. (Available from ASTIA.)

4. Mixson, John S., and Herr, Robert W.: An Investigation of the Vibration Characteristics of Pressurized Thin-Walled Circular Cylinders Partly Filled With Liquid. NASA TR R-145, 1962.

5. Weingarten, V. I.: Free Vibration of Thin Cylindrical Shells. AIAA Jour., vol. 2, no. 4, Apr. 1964, pp. 717-722.

6. Heckl, Manfred: Vibrations of Point-Driven Cylindrical Shells. Jour. Acoustical Soc. of America, vol. 34, no. 10, Oct. 1962, pp. 1553-1557.

7. Hoppmann, W. H., 2nd: Bending of Orthogonally Stiffened Plates. Jour. Appl. Mech., vol. 22, no. 2, June 1955, pp. 267-271.

8. Hoppmann, W. H., II: Elastic Compliances of Orthogonally Stiffened Plates. Tech. Rep. No. 9 (Navy Contract Nonr - 248(12)), The Johns Hopkins Univ. Inst. for Cooperative Res., Dept. Mech. Eng., July 1955.

9. Timoshenko, S., and Goodier, J. N.: Theory of Elasticity. McGraw-Hill Book Co., Inc., c.1951.

10. Bodner, S. R.: General Instability of a Ring-Stiffened Circular Cylindrical Shell Under Hydrostatic Pressure. Jour. Appl. Mech., vol. 24, no. 2, June 1957, pp. 269-277.

11. Biezeno, C. B., and Koch, J. J.: The Effective Width of Cylinders, Periodically Stiffened by Circular Rings. Proc. Koninklyke Nederlandsche Akademie van Wetenschappen (Netherlands), vol. XLVIII, 1945, pp. 147-165.

12. Galletly, Gerard D.: On the In-Vacuo Vibrations of Simply Supported, Ring-Stiffened Cylindrical Shells. Proc. Second U.S. National Congress of Appl. Mech., ASME, c.1955.

13. Hoppmann, W. H., II: Flexural Vibrations of Orthogonally Stiffened Cylindrical Shells. Tech. Rep. No. 11 (Contract Nonr-248(12)), Dept. Mech. Eng., The Johns Hopkins Univ., July 1956.

14. Nelson, H. C., Zapotowski, B., and Bernstein, M.: Vibration Analysis of Orthogonally Stiffened Circular Fuselage and Comparison with Experiment. National Specialists Meeting, Proc. Dynamics and Aeroelasticity, IAS (Fort Worth, Texas), Nov. 1958, pp. 77-87.

15. Miller, P. R.: Free Vibrations of a Stiffened Cylindrical Shell. R. & M. No. 3154, British A.R.C., 1960.

16. Grinsted, B.: Communications on the Flexural Vibrations of Thin Cylinders. Proc. Inst. Mech. Eng., vol. 167, no. 1, 1953, pp. 75-77.

17. Herr, Robert W.: A Wide-Frequency-Range Air-Jet Shaker. NACA TN 4060, 1957.

18. Brooks, George W.: Techniques for Simulation and Analysis of Shock and Vibration Environments of Space Flight Systems. Experimental Techniques in Shock and Vibration, Will J. Worley, ed., ASME, c.1962, pp. 93-105.

19. Lindholm, Ulric S., Kana, Daniel D., and Abramson, H. Norman: Breathing Vibrations of a Circular Cylindrical Shell With an Internal Liquid. Jour. Aerospace Sci., vol. 29, no. 9, Sept. 1962, pp. 1052-1059.

20. Thompson, William M., and Clary, Robert R.: An Investigation of the Natural Frequencies and Mode Shapes of Double Conical Sandwich Disks. NASA TN D-1940, 1963.

21. Tobias, S. A.: A Theory of Imperfection for the Vibrations of Elastic Bodies of Revolution. Engineering, vol. 172, no. 4470, Sept. 28, 1951, pp. 409-410.

22. Love, A. E. H.: A Treatise on the Mathematical Theory of Elasticity. 4th ed. (First Am. Printing), Dover Pub., 1944.

23. Rayleigh, (Lord): The Theory of Sound. First Am. ed. (Second ed. revised), vol. I, Dover Pub., 1945.

24. Young, Dana, and Felgar, Robert P., Jr.: Tables of Characteristic Functions Representing Normal Modes of Vibration of a Beam. Pub. No. 4913, Eng. Res. Ser. No. 44, Bur. Eng. Res., Univ. of Texas, July 1, 1949.

25. Felgar, Robert P., Jr.: Formulas for Integrals Containing Characteristic Functions of a Vibrating Beam. Cir. No. 14, Bur. Eng. Res., Univ. of Texas, 1950.

26. Timoshenko, S.: Vibration Problems in Engineering. 3rd ed., D. Van Nostrand Co., Inc., 1955.

TABLE I.- EFFECT OF POSITION AND TYPE OF SHAKER ON THE NATURAL FREQUENCIES

OF THE SINGLE-WALL MODEL WITH FREE ENDS

m	n	Natural frequency, cps, for -		
		Electromagnetic shaker on middle ring	Electromagnetic shaker on end ring	Air shaker on end ring
0	2	118	117	118
0	3	307	309	310
0	4	529	534	539
0	4	593	---	---
1	2	113	112	114
1	3	319	315	320
1	4	561	552	560
1	4	---	606	---
1	5	---	784	---
2	4	658	659	651
2	5	790	---	---
2	5	826	834	---
2	5	866	865	---

TABLE II.- EFFECT OF OUTER SHELL ATTACHMENT ON NATURAL FREQUENCIES

OF FREE-ENDED MODEL

m	n	Natural frequency, cps, for -		
		Inner shell only	Outer shell riveted	Outer shell riveted and welded
0	2	117	109	116
0	3	309	288	315
0	4	534	492	548
1	2	112	119	126
1	3	315	311	331
1	4	552	543	574
1	4	606	---	610
1	5	784	---	---
2	4	659	[a]630	---
2	4	---	713	732
2	5	834	---	---
2	5	865	---	---

[a]Weak response.

TABLE III.- NATURAL FREQUENCIES OF THE MODEL WITH ONE END FIXED

AND WITH AND WITHOUT OUTER SHELL INSTALLED

m	n	Natural frequency, cps, for -			
		Inner shell only	Outer shell riveted	Outer shell riveted and welded	Outer shell riveted and welded, spider in free end
1	1	--------------	---	157	185
1	2	169; 196	143	146	302; 317
1	3	321	301	319	412; 456
1	4	504; 545	508	551	560; 612
2	2	752	---	--------	--------
2	3	574	597	--------	--------
2	4	607; 644; 686	623	606; 663	689
2	5	803	---	--------	--------

TABLE IV.- NATURAL FREQUENCIES OF THE MODEL WITH FIXED-FIXED CONDITIONS

AND WITH AND WITHOUT THE OUTER SHELL INSTALLED

m	n	Natural frequency, cps, for -	
		Inner shell only	Outer shell riveted
1	2	--------------------	579; 608
1	3	378; 395; 410; 441; 463; 488; 507	465; 494
1	4	580; 600	555; 591
1	5	760	706
2	3	419	--------

TABLE V.- NATURAL FREQUENCIES OF THE MODEL WITH ONE END FIXED AND MOUNTED ON

LONGITUDINAL SUPPORTS, WITH AND WITHOUT THE OUTER SHELL INSTALLED

m	n	Natural frequency, cps, for -		
		Inner shell only	Outer shell riveted and welded	Outer shell riveted and welded, spider in free end
1	1	---------	--------------------	121; 158; 186
1	2	236; 279	136; 174; 193; 205; 211; 226	211; 245; 269; 305
1	3	334; 354; 360; 387	--------------------	374; 409; 467; 535

TABLE VI.- PROPERTIES OF LONGITUDINAL COMPONENTS OF MODE SHAPES OF CYLINDRICAL SHELLS WITH VARIOUS END CONDITIONS

(a) Functions and integrals

End condition	m	$X_m(x)$	$\int_0^L X_m{}^2\,dx$	$\int_0^L (X_m')^2\,dx$	$\int_0^L (X_m'')^2\,dx$	$\int_0^L X_m X_m''\,dx$
Free-free	0	1	L	0	0	0
	1	$\dfrac{x}{L} - \dfrac{1}{2}$	$\dfrac{L}{12}$	$\dfrac{1}{L}$	0	0
	$\geqq 2$	$\cosh N_m x + \cos N_m x - \gamma_m\left(\sinh N_m x + \sin N_m x\right)$	L	$\gamma_m N_m\left(\gamma_m N_m L + 6\right)$	$N_m{}^4 L$	$-\gamma_m N_m\left(\gamma_m N_m L - 2\right)$
Cantilever (at $x = 0$)	1	$\left(\dfrac{x}{L}\right)^2$	$\dfrac{L}{5}$	$\dfrac{4}{3L}$	$\dfrac{4}{L^3}$	$\dfrac{2}{3L}$
	$\geqq 1$	$\cosh N_m x - \cos N_m x - \gamma_m\left(\sinh N_m x - \sin N_m x\right)$	L	$\gamma_m N_m\left(\gamma_m N_m L + 2\right)$	$N_m{}^4 L$	$-\gamma_m N_m\left(\gamma_m N_m L - 2\right)$
Supported-sliding[*]	$\geqq 1$	$\cos\left[\left(\dfrac{2m - 1}{2}\right)(\pi)\left(\dfrac{x}{L} - 1\right)\right]$	$\dfrac{L}{2}$	$\dfrac{(2m - 1)^2\pi^2}{8L}$	$\dfrac{(2m - 1)^4\pi^4}{32L^3}$	$-\dfrac{(2m - 1)^2\pi^2}{8L}$
Clamped-clamped	$\geqq 1$	$\cosh N_m x - \cos N_m x - \gamma_m\left(\sinh N_m x - \sin N_m x\right)$	L	$\gamma_m N_m\left(\gamma_m N_m L - 2\right)$	$N_m{}^4 L$	$-\gamma_m N_m\left(\gamma_m N_m L - 2\right)$
Simply supported	$\geqq 1$	$\sin\dfrac{m\pi x}{L}$	$\dfrac{L}{2}$	$\dfrac{(m\pi)^2}{2L}$	$\dfrac{(m\pi)^4}{2L^3}$	$-\dfrac{(m\pi)^2}{2L}$

[*] Supported end at $x = 0$.

(b) Values of parameters N_m and γ_m (from ref. 24)

m Clamped ends	Free ends	$N_m L$	γ_m	m	Cantilevered shell $N_m L$	γ_m
1	2	4.7300408	0.9825022158	1	1.8751041	0.7340955
2	3	7.8532046	1.00077731	2	4.69409113	1.018466644
3	4	10.9956078	.9999664501	3	7.85475743	.99922450
4	5	14.1371655	1.000001450	4	10.99554074	1.000033553
5	6	17.2787596	.9999999373	5	14.13716839	.9999985501
>5	---	$(2m + 1)\pi/2$	1	>5	$(2m - 1)\pi/2$	1
---	>6	$(2m - 1)\pi/2$				

Equations for $N_m L$ and γ_m:

$$\cosh N_m L \cos N_m L = 1 \qquad\qquad \cosh N_m L \cos N_m L = -1$$

$$\gamma_m = \frac{\cosh N_m L - \cos N_m L}{\sinh N_m L - \sin N_m L} \qquad\qquad \gamma_m = \frac{\cosh N_m L + \cos N_m L}{\sinh N_m L + \sin N_m L}$$

TABLE VII.- COMPARISON OF THEORY AND EXPERIMENT FOR TWO LOWEST FREE-FREE

NATURAL FREQUENCIES BASED ON TWO APPROXIMATIONS OF EFFECTIVE LENGTH

OF SHELL FOR EACH RING STIFFENER

(a) Double-walled shell structure (See also fig. 11.)

n	Experimental frequency, cps	Theoretical frequency, cps, for -	
		$\dfrac{\overline{L}_{x,i}}{L_x} = 0.272$ $\dfrac{\overline{L}_{x,o}}{L_x} = 0.2805$ (*)	$\dfrac{\overline{L}_{x,i}}{L_x} = 1.0$ $\dfrac{\overline{L}_{x,o}}{L_x} = 1.0$
		m = 0	
2	116	115	179
3	315	325	507
4	548	623	972
5	---	1,008	1,571
		m = 1	
2	126	188	227
3	331	443	586
4	574; 610	764	1,065
5	--------	1,161	-----

(b) Single-walled shell structure (See also fig. 12.)

n	Experimental frequency, cps (**)	Theoretical frequency, cps, for -	
		$\dfrac{\overline{L}_{x,i}}{L_x} = 0.272$ (*)	$\dfrac{\overline{L}_{x,i}}{L_x} = 1.0$
		m = 0	
2	117.5	121	141
3	309.5	341	398
4	536.5	653	764
5	-----	1,056	1,235
		m = 1	
2	113	112	132
3	317.5	335	392
4	556; 606	650	760
5	784	1,054	1,233

*These effective length ratios based on approximation given in reference 12.

**Experimental frequencies are average values based on air shaker and electromagnetic shaker.

TABLE VIII.- COMPARISON OF EXPERIMENTAL AND THEORETICAL SHELL FREQUENCIES WITH

RING FREQUENCIES FOR FREE-ENDED SHELL STRUCTURES WITH $m = 0$

(a) Ring-stiffened shell structure
(See figs. 11 and 12.)

(b) Unstiffened shell (See fig. 9.)

n	Experimental frequency, cps	Theoretical frequency, cps, for -	
		Shell*	Ring
Double wall			
2	116	115	112.4
3	315	325	317.7
4	548	623	610
5	----	1,008	984
Single wall			
2	117.5	121	112
3	309.5	341	316.5
4	536.5	653	607
5	-----	1,056	981

n	Experimental frequency, cps	Theoretical frequency, cps, for -	
		Shell	Ring
2	200	262	250.9
3	700	744	709
4	1,350	1,426	1,360
5	2,050	2,306	2,199

*Double wall:

$$\frac{\bar{L}_{x,i}}{L_x} = 0.272; \quad \frac{\bar{L}_{x,o}}{L_x} = 0.2805$$

Single wall:

$$\frac{\bar{L}_{x,i}}{L_x} = 0.272$$
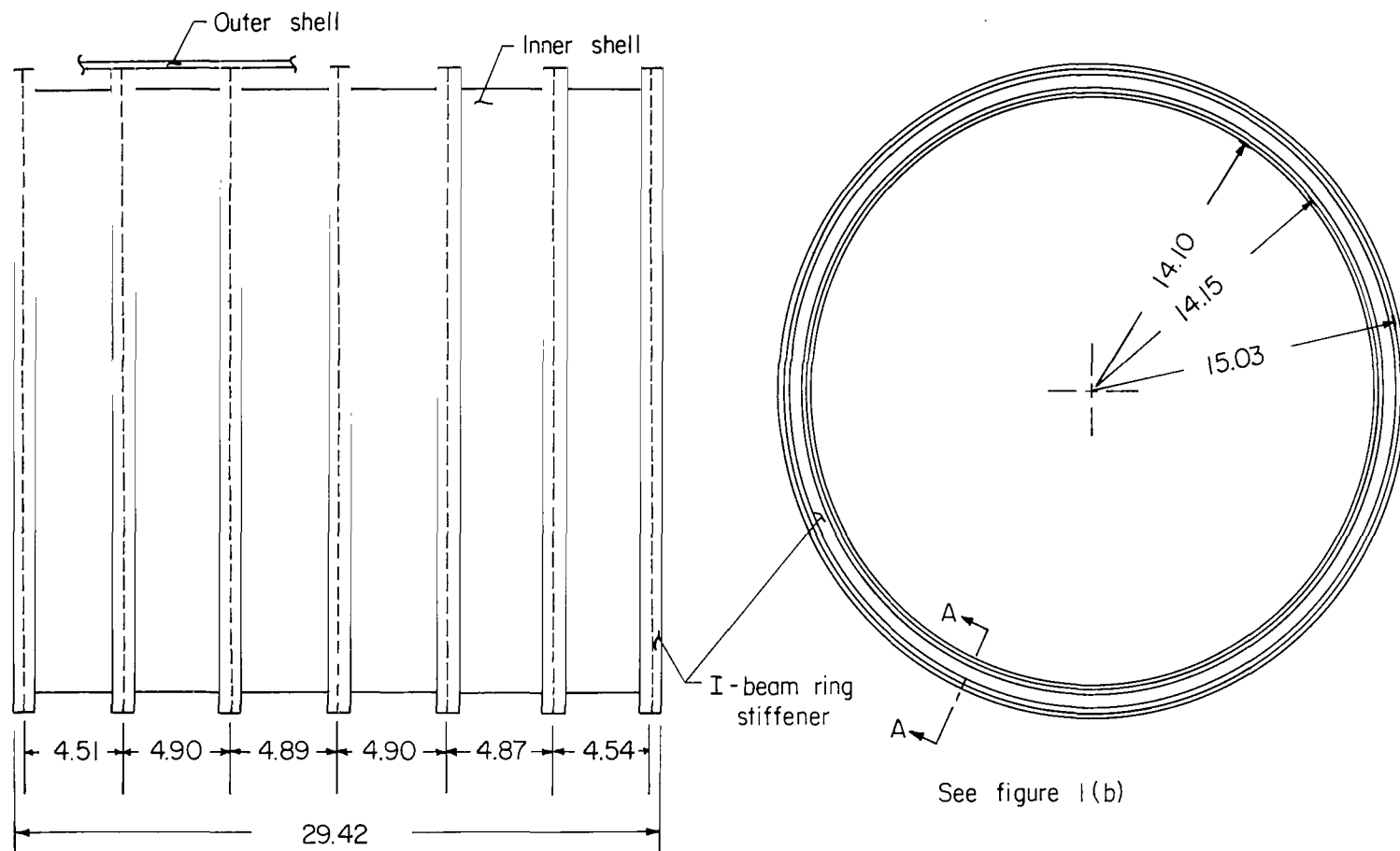
(a) Arrangement of rings and shells.

Figure 1.- Structural details of ring-stiffened cylindrical shell model. (All dimensions are in inches.)
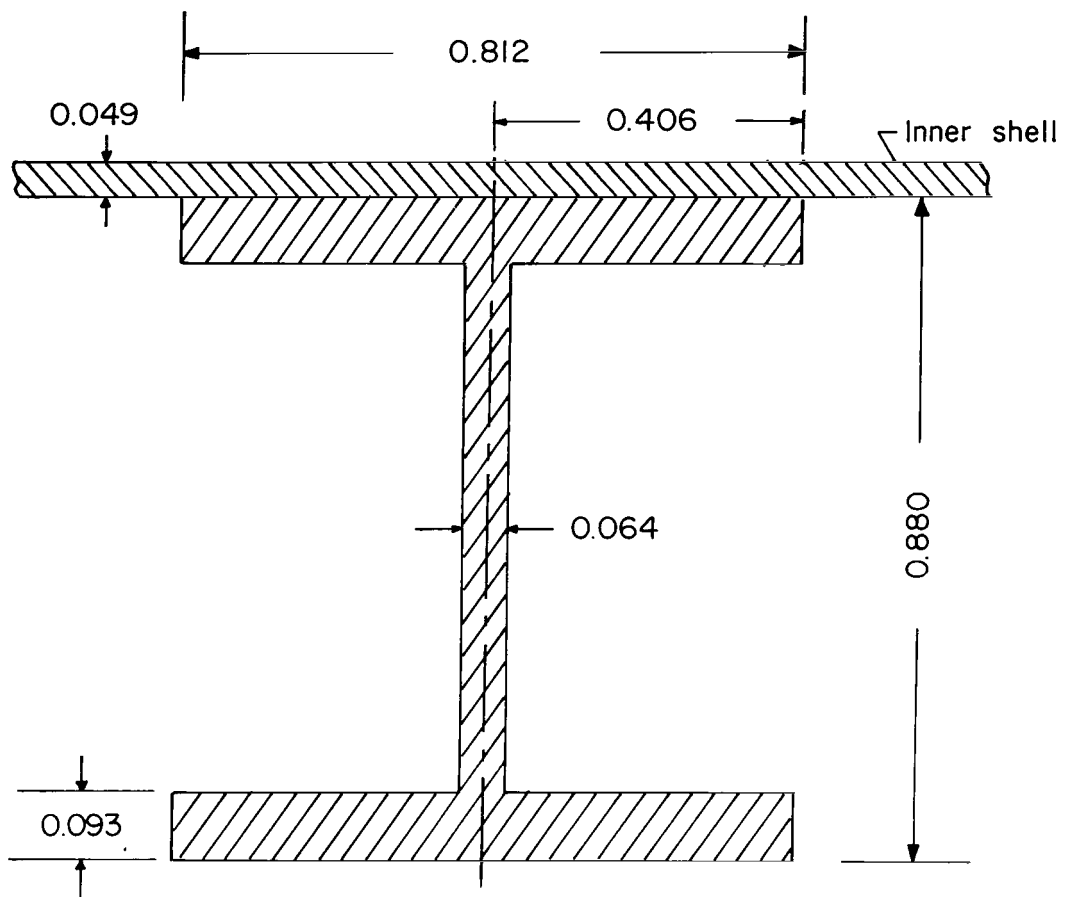
(b) Cross-sectional details of I-beam ring stiffeners.

Figure 1.- Concluded.
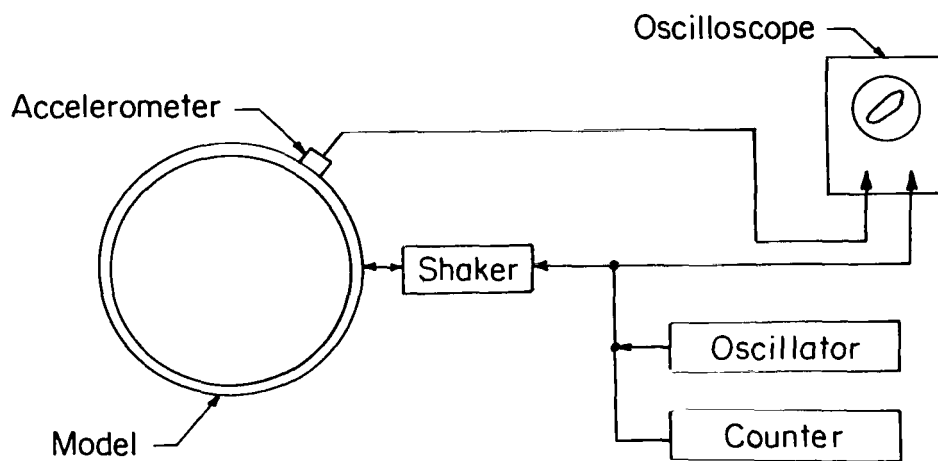
Figure 2.- Block diagram of instrumentation used with electromagnetic shaker.

Clamping dogs

(a) Single-wall model.

Clamping dogs
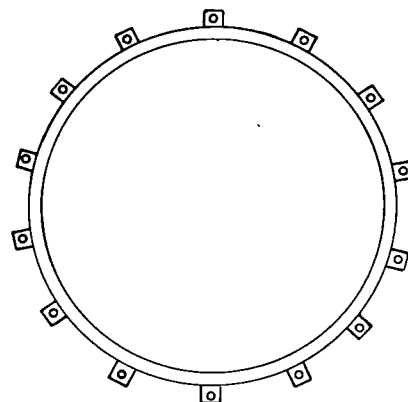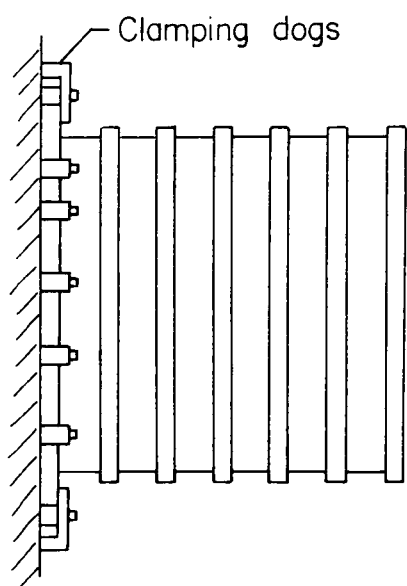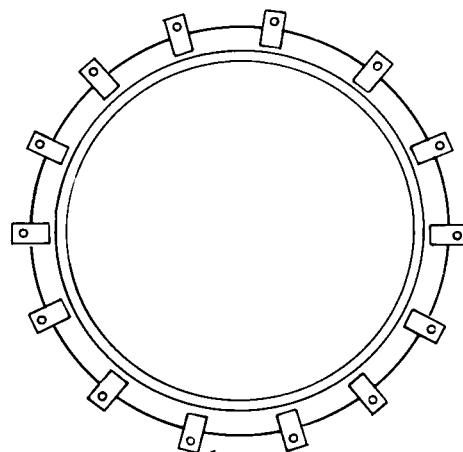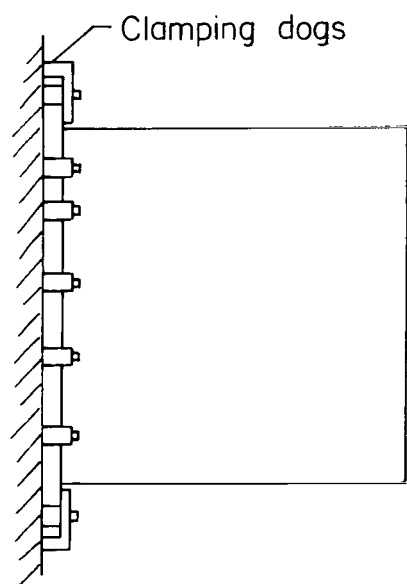
(b) Double-wall model.

Figure 3.- Mounting system for model with fixed-free end conditions.
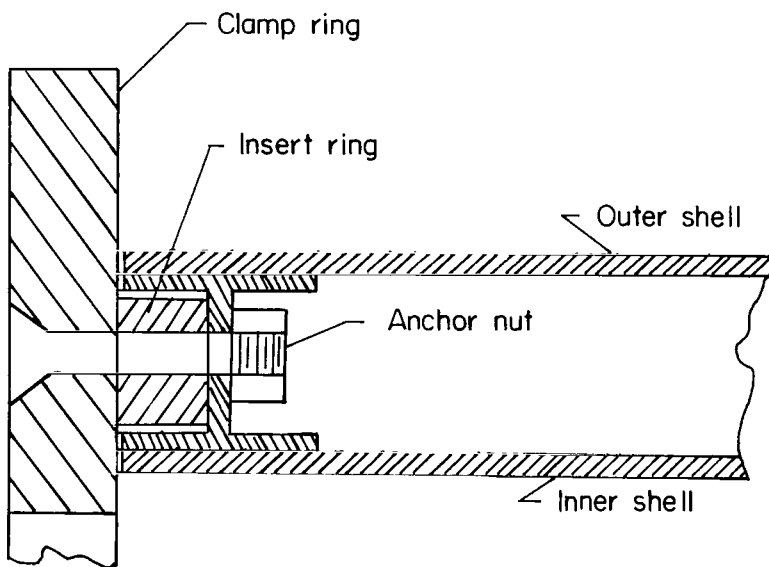
(a) End attached to backstop.
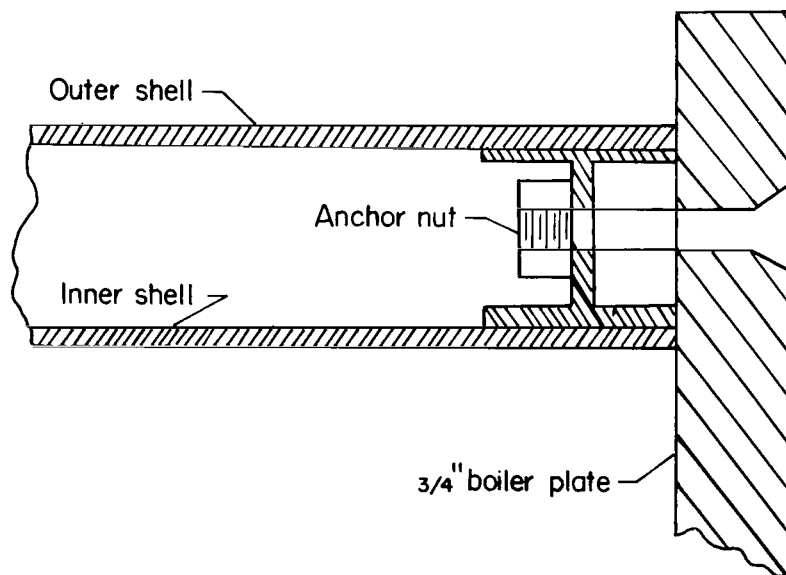
(b) End attached to boiler plate.

Figure 4.- Details of end conditions for double-wall model.
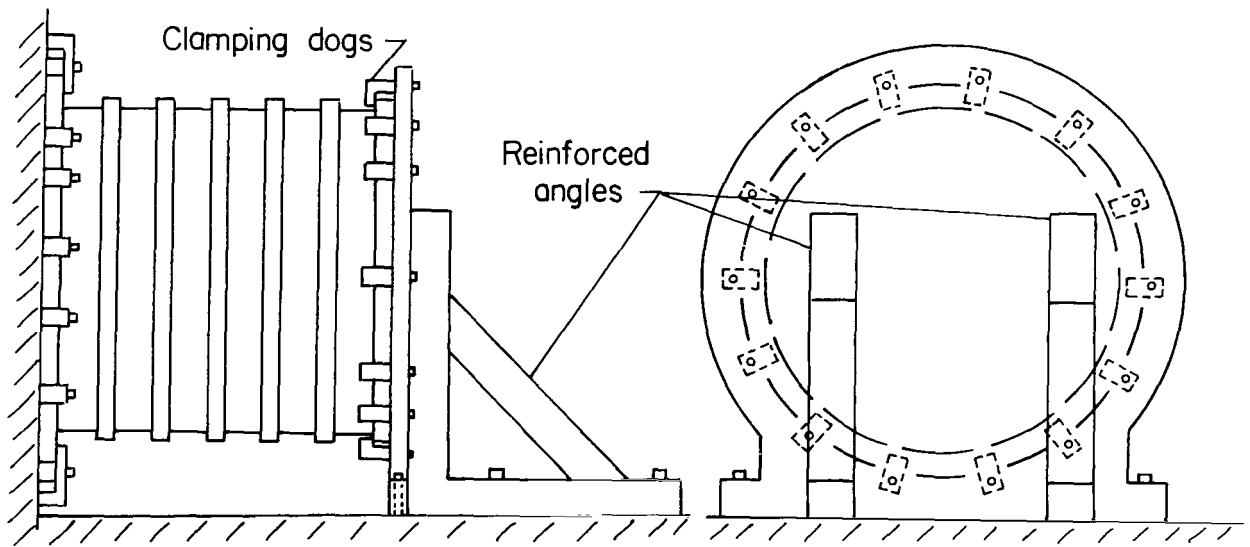
(a) Single-wall model.
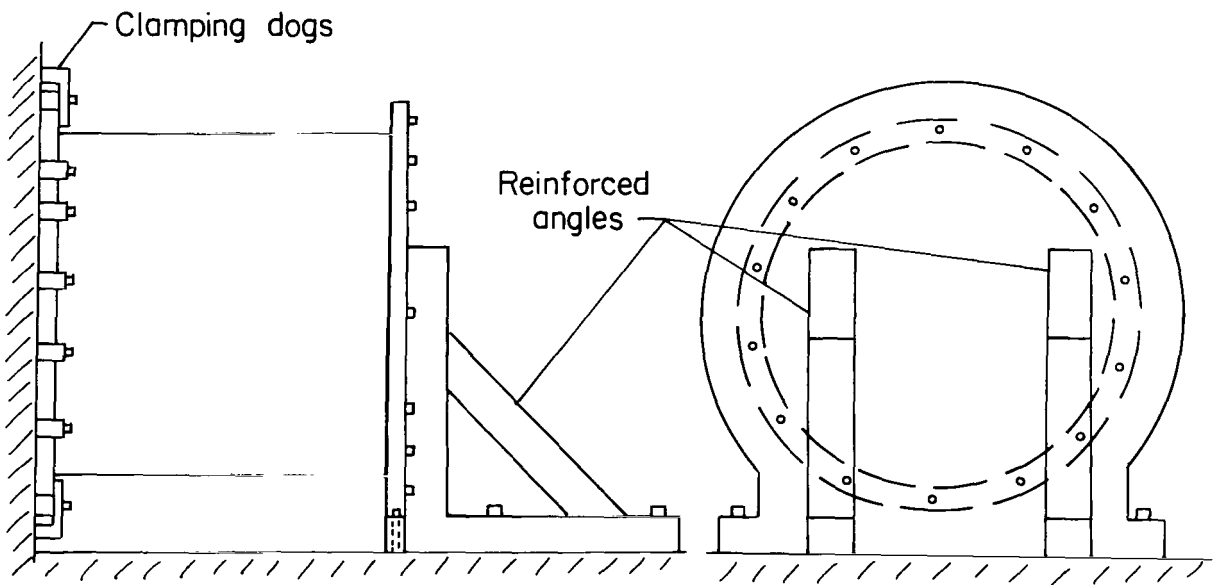
(b) Double-wall model.

Figure 5.- Mounting system for model with both ends fixed.
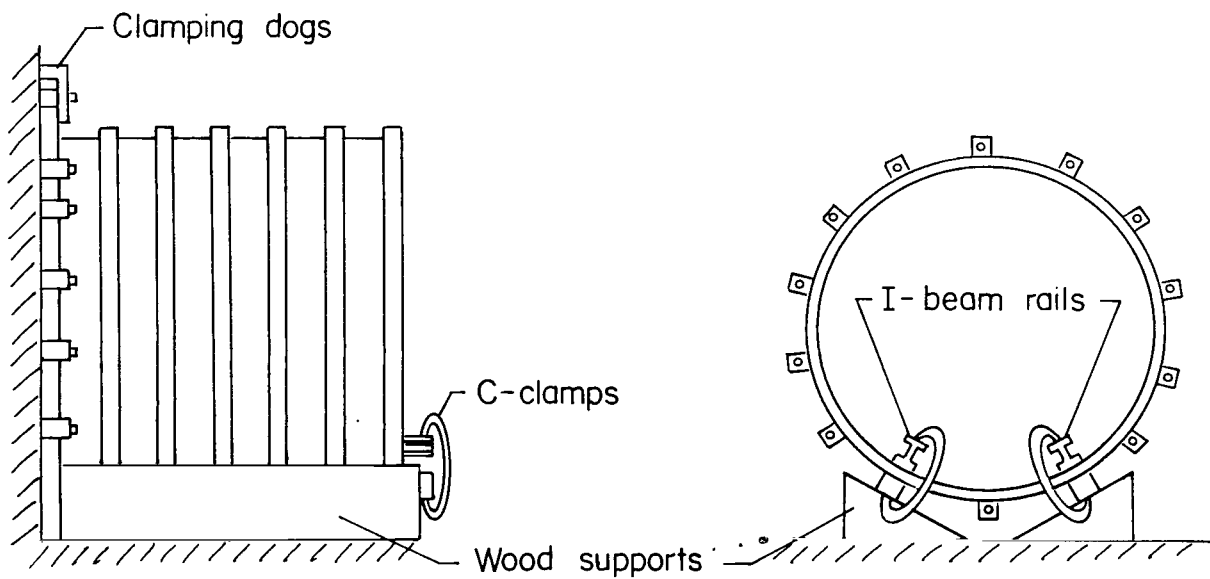
(a) Single-wall model.
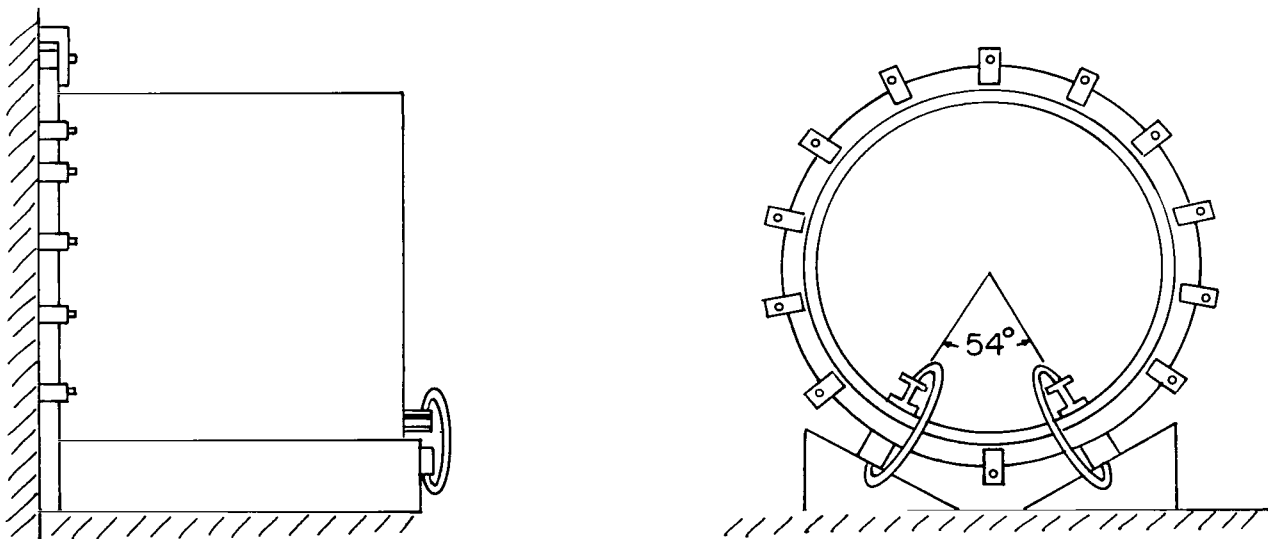
(b) Double-wall model.

Figure 6.- Mounting system for model with one end fixed and supported longitudinally.
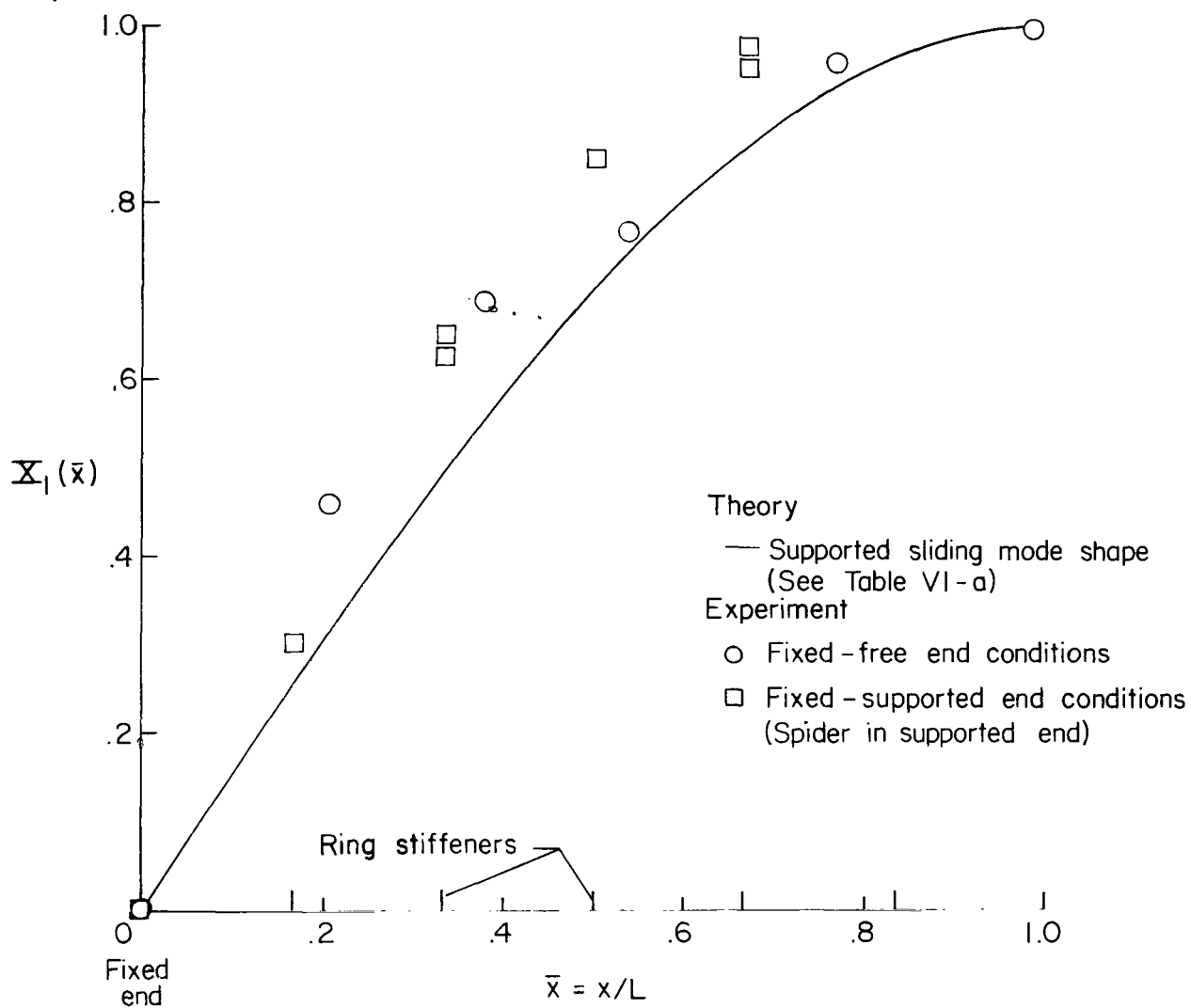
Figure 7.- Comparison of measured and calculated longitudinal mode shapes of double-wall ring-stiffened cylindrical shell with one end fixed. $X_1(\bar{x}) = \cos\left[\frac{\pi}{2}(\bar{x} - 1)\right]$.
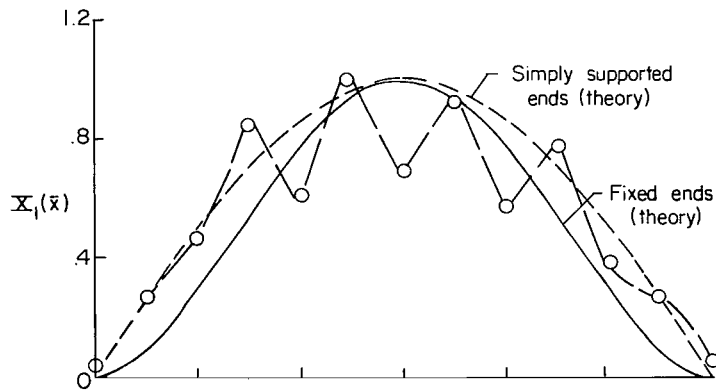
(a) f_{13} = 395 cps.
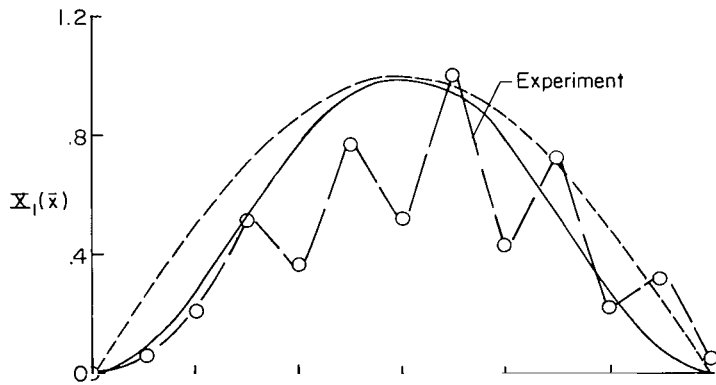
(b) f_{14} = 580 cps.
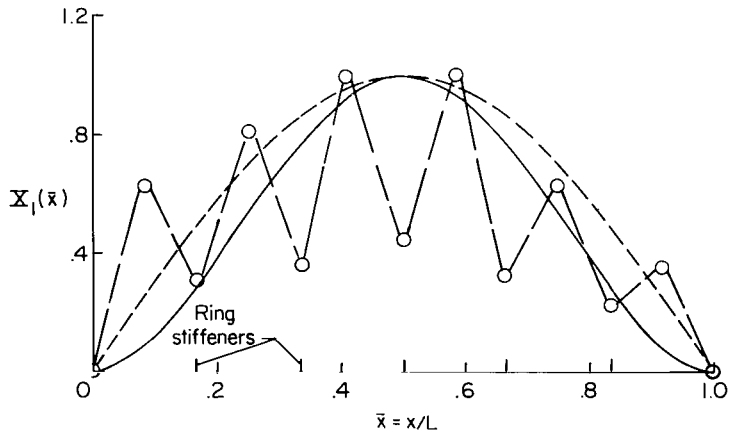
(c) f_{15} = 760 cps.

Figure 8.- Comparison of measured and calculated longitudinal mode shapes of single-wall ring-stiffened cylindrical shell with fixed ends. Backstop located at station $\bar{x}$ = 0.
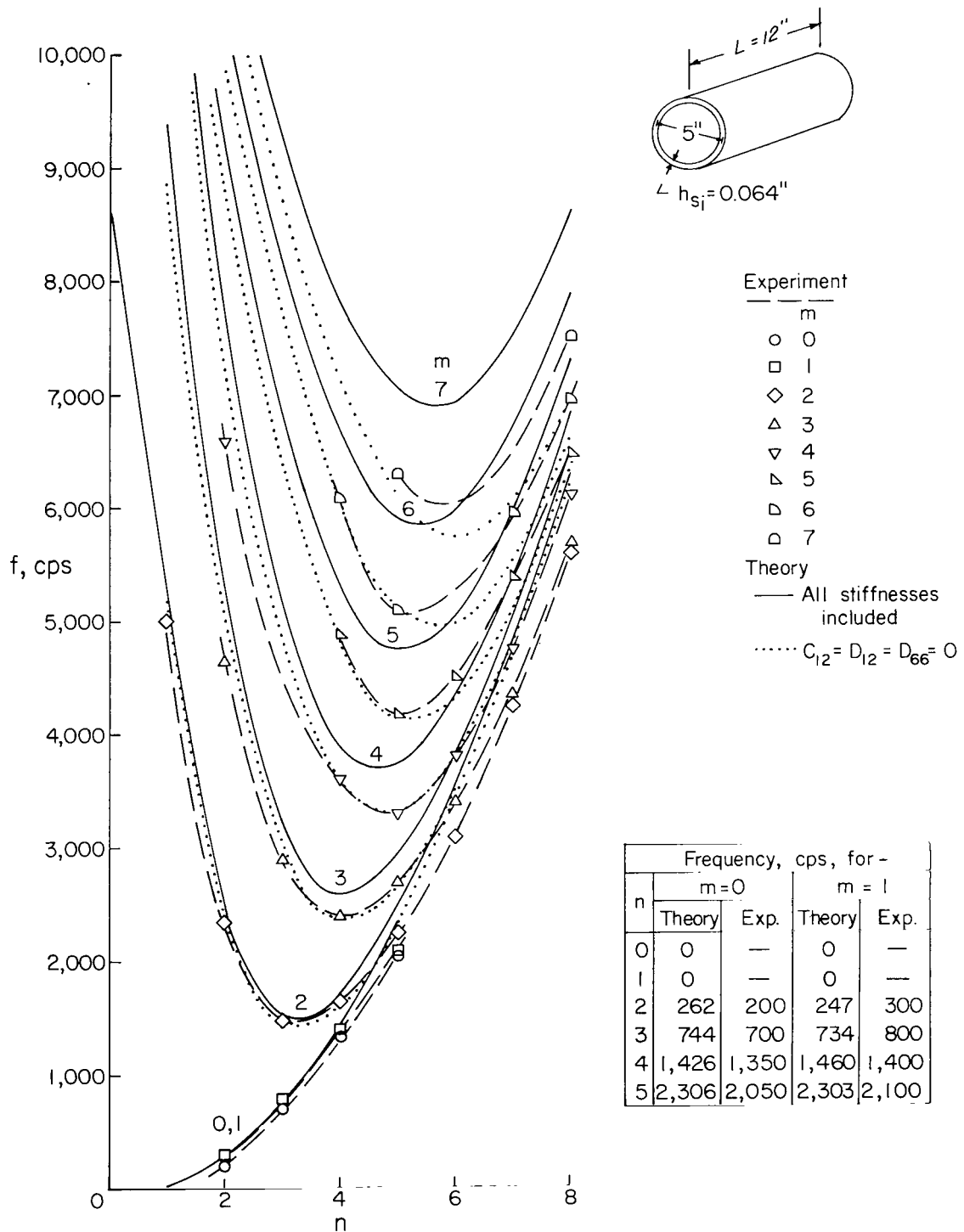
Figure 9.- Theoretical and experimental frequencies of free-ended, unstiffened, steel cylindrical shell. (Experimental frequencies were obtained from ref. 16.)
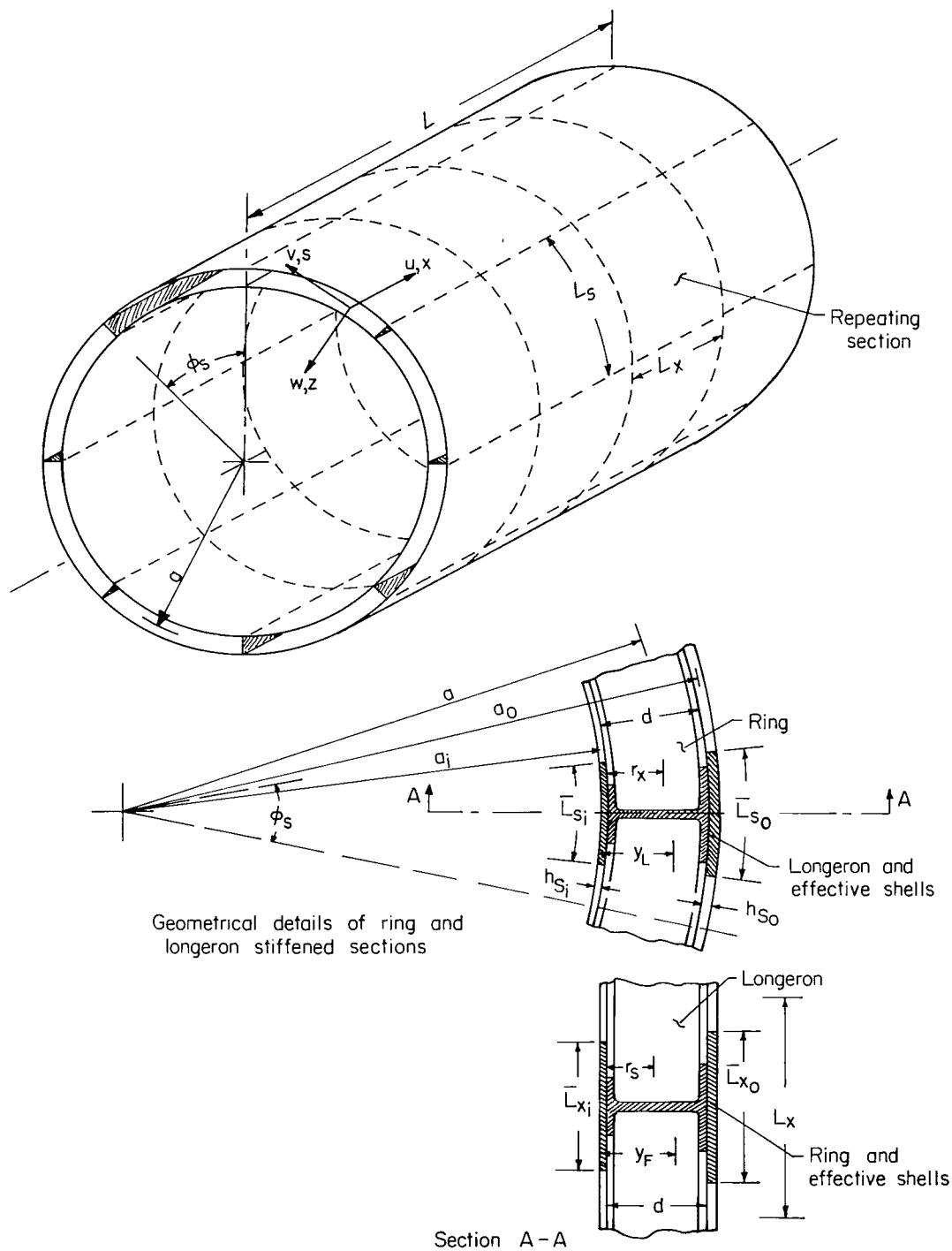
Figure 10.- Analytical vibration model of orthogonally stiffened double-walled cylindrical shell structure.
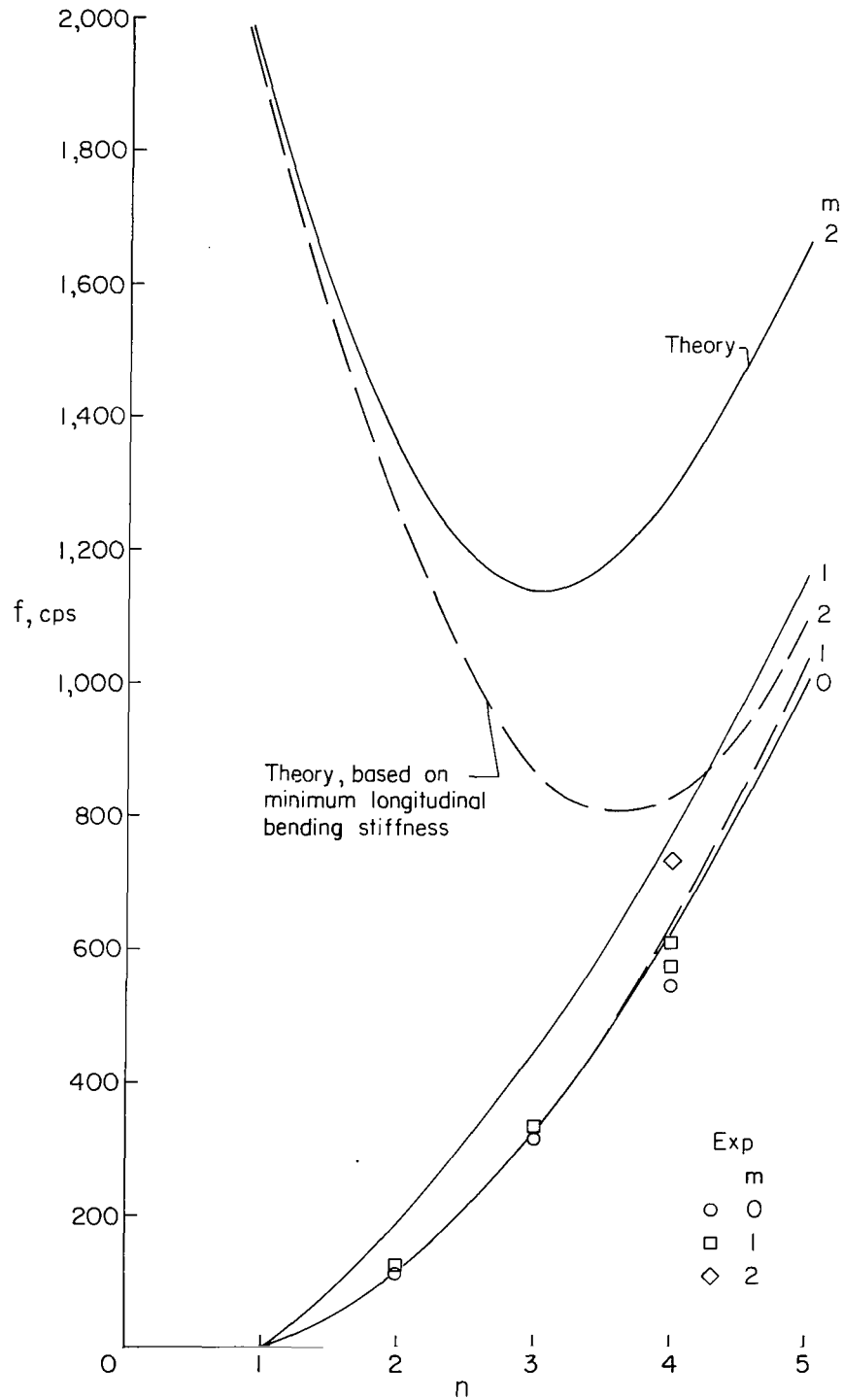
Figure 11.- Theoretical and experimental frequencies of free-ended, ring-stiffened double-walled steel cylindrical shell.
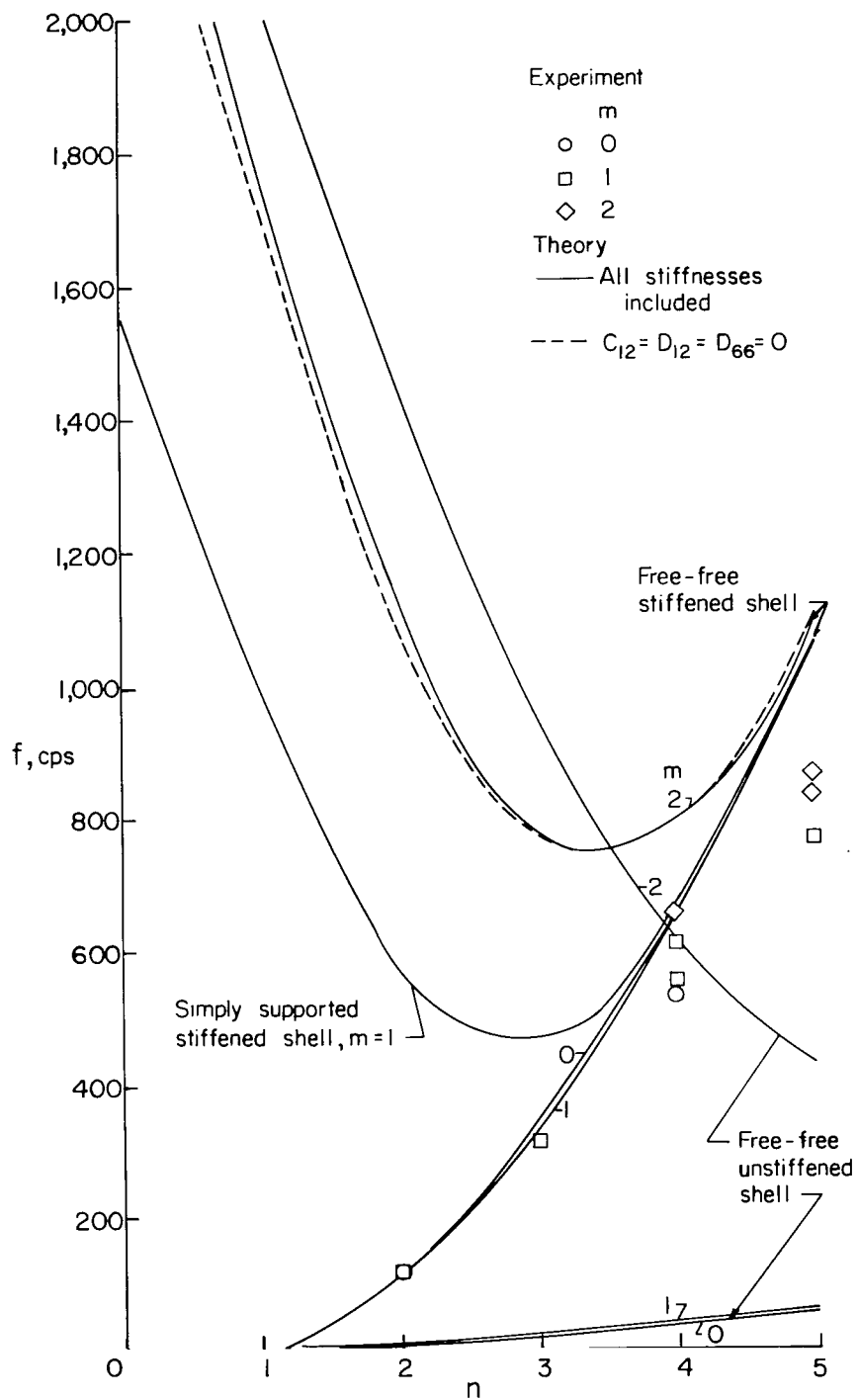
Figure 12.- Theoretical and experimental frequencies of free-ended, ring-stiffened single-walled steel cylindrical shell.
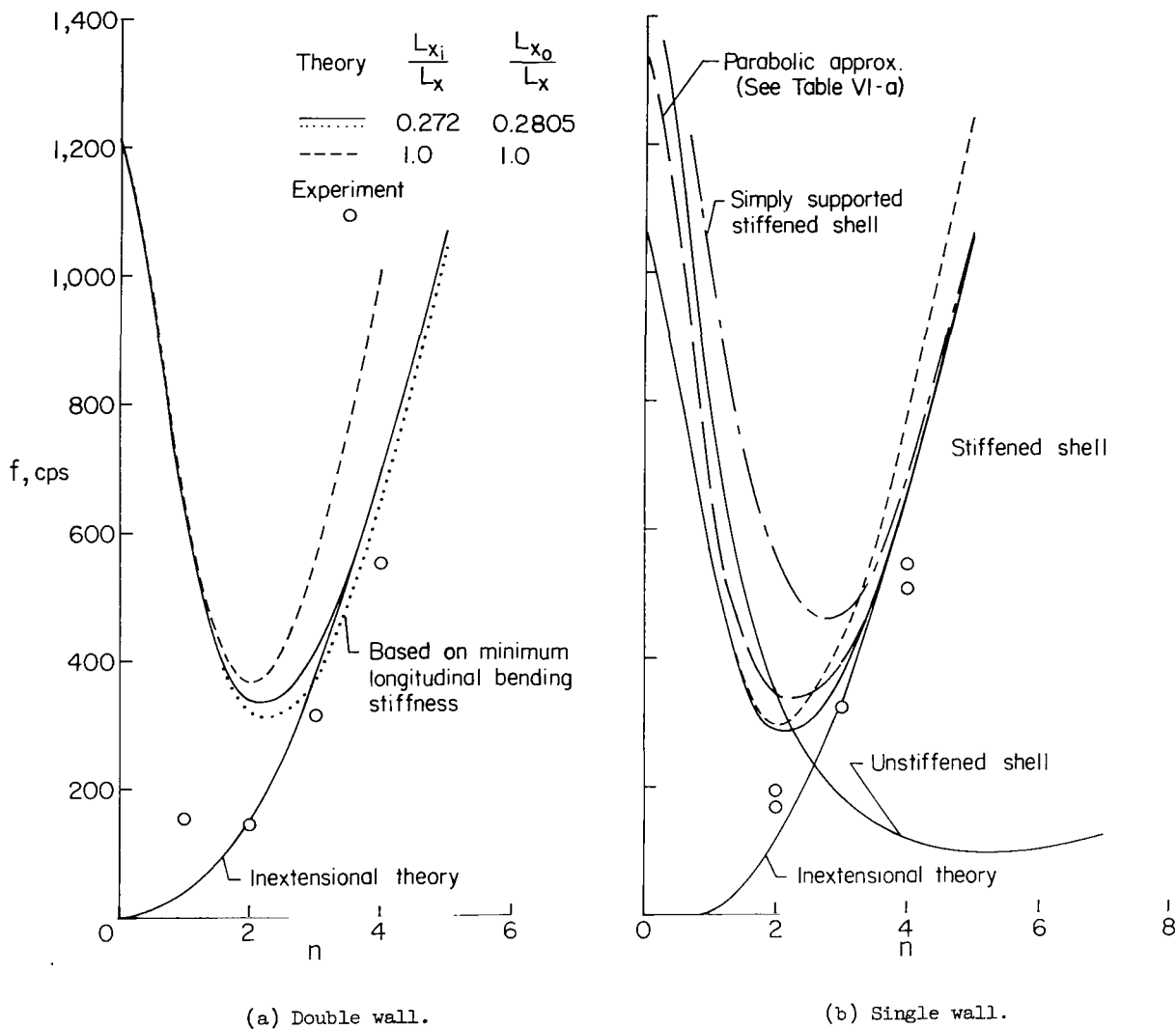
(a) Double wall.   (b) Single wall.

Figure 13.- Theoretical and experimental frequencies of ring-stiffened steel cylindrical shells
cantilevered at one end and free at the other for m = 1. Circular symbols denote experi-
mental values, and the curves represent theoretical values which are based on beam mode
approximations except as noted in figure 13(b).
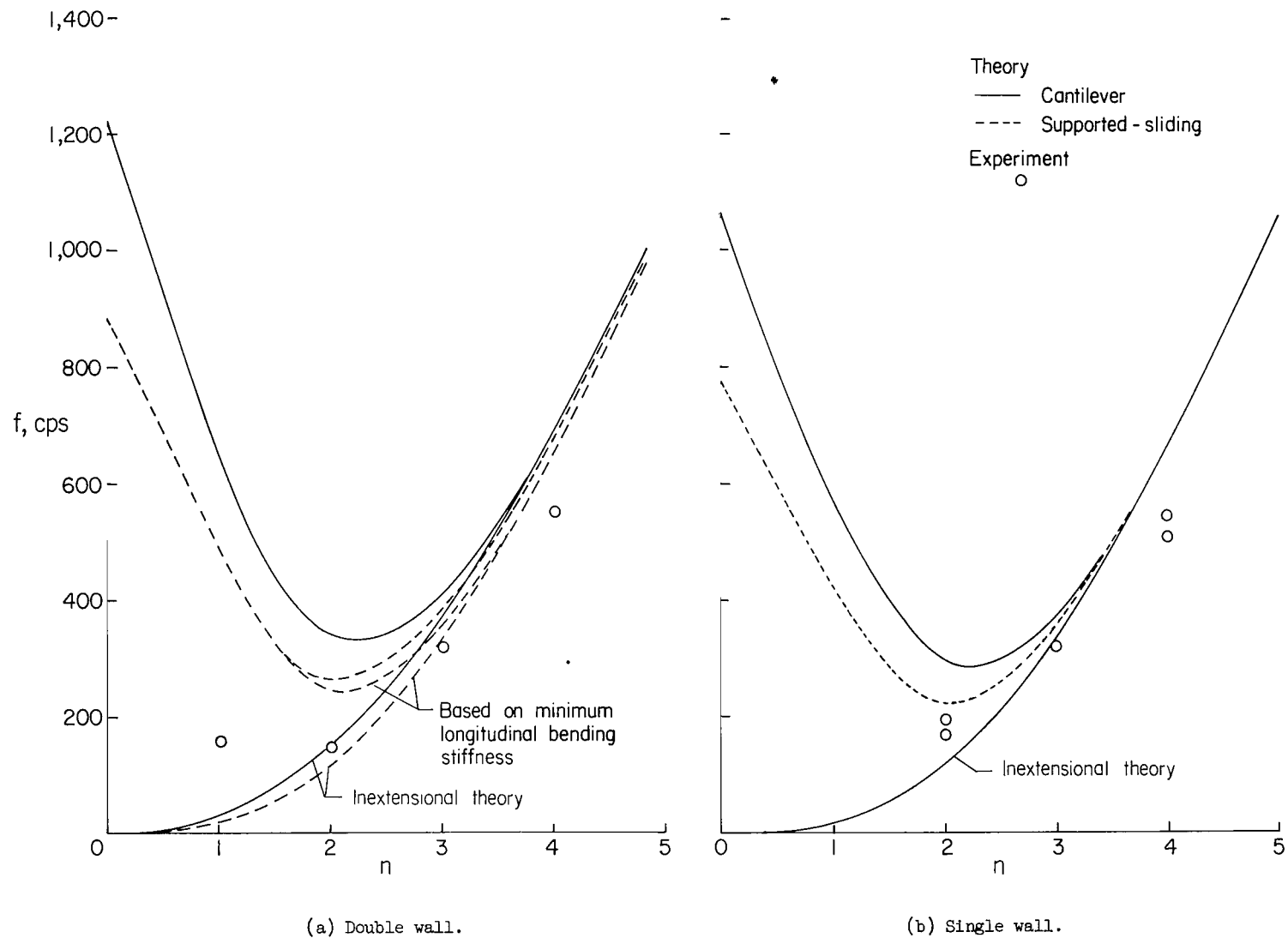
(a) Double wall.   (b) Single wall.

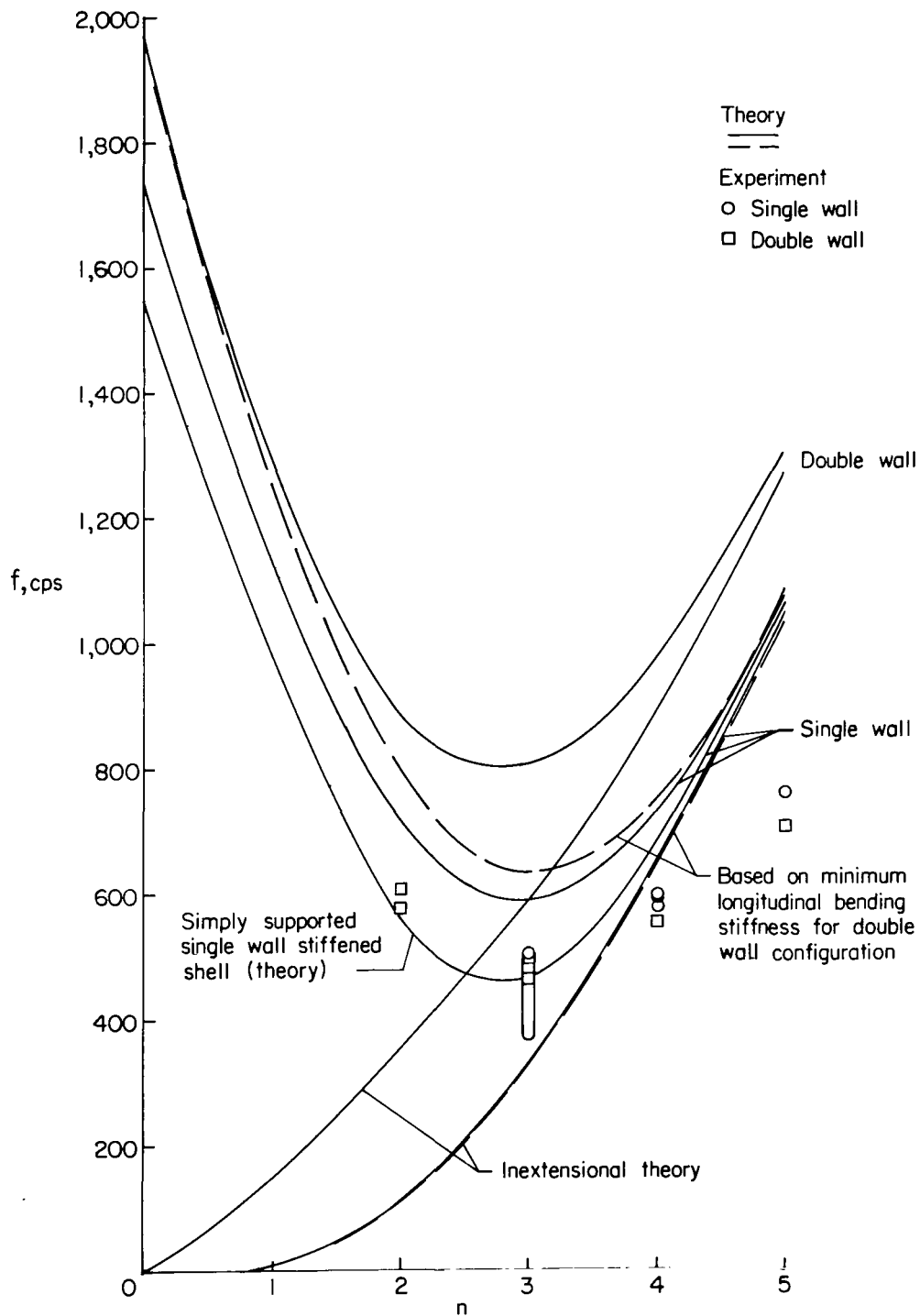Figure 14.- Comparison of theoretical and experimental frequencies of cantilever and supported-sliding end conditions.
m = 1.

Figure 15.- Theoretical and experimental frequencies of ring-stiffened steel cylindrical shell clamped at both ends. m = 1.

> "The aeronautical and space activities of the United States shall be conducted so as to contribute . . . to the expansion of human knowledge of phenomena in the atmosphere and space. The Administration shall provide for the widest practicable and appropriate dissemination of information concerning its activities and the results thereof."
>
> —NATIONAL AERONAUTICS AND SPACE ACT OF 1958

NASA SCIENTIFIC AND TECHNICAL PUBLICATIONS

TECHNICAL REPORTS: Scientific and technical information considered important, complete, and a lasting contribution to existing knowledge.

TECHNICAL NOTES: Information less broad in scope but nevertheless of importance as a contribution to existing knowledge.

TECHNICAL MEMORANDUMS: Information receiving limited distribution because of preliminary data, security classification, or other reasons.

CONTRACTOR REPORTS: Technical information generated in connection with a NASA contract or grant and released under NASA auspices.

TECHNICAL TRANSLATIONS: Information published in a foreign language considered to merit NASA distribution in English.

TECHNICAL REPRINTS: Information derived from NASA activities and initially published in the form of journal articles.

SPECIAL PUBLICATIONS: Information derived from or of value to NASA activities but not necessarily reporting the results of individual NASA-programmed scientific efforts. Publications include conference proceedings, monographs, data compilations, handbooks, sourcebooks, and special bibliographies.

Details on the availability of these publications may be obtained from:

SCIENTIFIC AND TECHNICAL INFORMATION DIVISION

NATIONAL AERONAUTICS AND SPACE ADMINISTRATION

Washington, D.C. 20546